AD-A147 177 A GENERAL THEORY OF CIRCUIT ANALOGY IN FRACTURE DIAGNOSIS(U) NEW MEXICO UNIV ALBUQUERQUE BUREAU OF ENGINEERING RESEARCH M AKGUN ET AL. MAR 84 1/1

UNCLASSIFIED ME124(84)AFOSR-993-1 AFOSR-TR-84-0910 F/G 14/2 NL

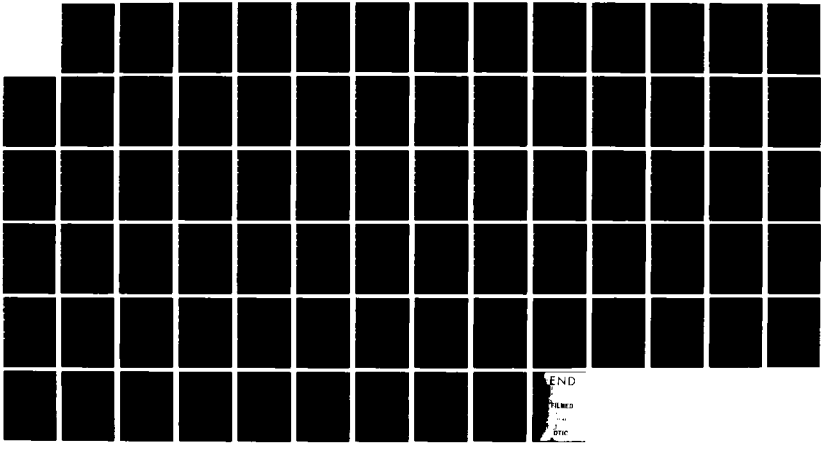

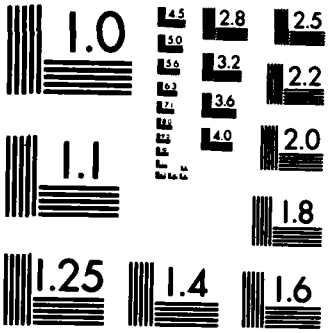

THE UNIVERSITY OF NEW MEXICO
COLLEGE OF ENGINEERING



# BUREAU OF ENGINEERING RESEARCH

Interim Report

## A GENERAL THEORY OF CIRCUIT ANALOGY IN FRACTURE DIAGNOSIS

by

Mehmet Akgün
Frederick D. Ju
Thomas L. Paez





ME124(84)AFOSR-993-1

Qualified requestors may obtain additional copies from the Defense Technical Information Service.

UNCLASSIFIED

SECURITY CLASSIFICATION OF THIS PAGE

## REPORT DOCUMENTATION PAGE

| | |
|---|---|
| 1a. REPORT SECURITY CLASSIFICATION: UNCLASSIFIED | 1b. RESTRICTIVE MARKINGS |
| 2a. SECURITY CLASSIFICATION AUTHORITY | 3. DISTRIBUTION/AVAILABILITY OF REPORT: Approved for Public Release; Distribution Unlimited. |
| 2b. DECLASSIFICATION/DOWNGRADING SCHEDULE | |
| 4. PERFORMING ORGANIZATION REPORT NUMBER(S): ME124(84)AFOSR-993-1 | 5. MONITORING ORGANIZATION REPORT NUMBER(S): AFOSR-TR- 84-0910 |
| 6a. NAME OF PERFORMING ORGANIZATION: University of New Mexico; 6b. OFFICE SYMBOL (If applicable): UNM | 7a. NAME OF MONITORING ORGANIZATION: AFOSR/NA |
| 6c. ADDRESS (City, State and ZIP Code): Bureau of Engineering Research, Albuquerque, NM 87131 | 7b. ADDRESS (City, State and ZIP Code): Bolling AFB, DC 20332 |
| 8a. NAME OF FUNDING/SPONSORING ORGANIZATION: Air Force Office of Scientific Research; 8b. OFFICE SYMBOL (If applicable): AFOSR/NA | 9. PROCUREMENT INSTRUMENT IDENTIFICATION NUMBER: AFOSR-81-0086 |
| 8c. ADDRESS (City, State and ZIP Code): Bolling AFB, DC 20332 | 10. SOURCE OF FUNDING NOS. |

| PROGRAM ELEMENT NO. | PROJECT NO. | TASK NO. | WORK UNIT NO. |
|---|---|---|---|
| 61102F | 2307 | C2 | |

11. TITLE (Include Security Classification): A General Theory of Circuit Analogy in Fracture Diagnosis (Unclassified)

12. PERSONAL AUTHOR(S): Mehmet Akgün, Frederick D. Ju, Thomas L. Paez

| 13a. TYPE OF REPORT | 13b. TIME COVERED | 14. DATE OF REPORT (Yr., Mo., Day) | 15. PAGE COUNT |
|---|---|---|---|
| Interim | FROM 15 Feb 83 TO 15Feb84 | 1984 March | 67 |

16. SUPPLEMENTARY NOTATION: Reproduction, translation, publication, use and disposal in whole or in part by or for the United States Government is permitted.

| 17. COSATI CODES | | |
|---|---|---|
| FIELD | GROUP | SUB. GR. |
| | | |
| | | |

18. SUBJECT TERMS (Continue on reverse if necessary and identify by block number): Damage diagnosis; Circuit analogy; Fracture hinge; Multiple cracks; Simple beams; Multi-story frame

19. ABSTRACT (Continue on reverse if necessary and identify by block number)

The present report develops electrical analogs to investigate multiple cracks on simple beams and more complex frame structures. Analog networks provide the economic tool to analyze such structures. The effect of multiple cracks on the natural frequencies of simple structures is studied in detail. It is shown that closely spaced multiple cracks are indistinguishable from an effective single crack. A severe crack on a structure can be identified if there are only minor cracks in addition to the major one. If, on the other hand, there is more than one severe crack, then the damage cannot, in general, be diagnosed with only three frequencies measurable. Nevertheless, a minimum number of cracks which are likely to be present in the structure can be established.

Characteristic equations are developed in the form of linear systems for cantilever beam and general frame structures with multiple cracks. Usefulness of relative-frequency-change curves are demonstrated and rough guidelines are provided to aid the damage diagnosis process. Several numerical examples are included which illustrate the effect of multiple cracks on frequencies.

| 20. DISTRIBUTION/AVAILABILITY OF ABSTRACT | 21. ABSTRACT SECURITY CLASSIFICATION |
|---|---|
| UNCLASSIFIED/UNLIMITED ☒ SAME AS RPT. ☐ DTIC USERS ☐ | Unclassified |

| 22a. NAME OF RESPONSIBLE INDIVIDUAL | 22b. TELEPHONE NUMBER (Include Area Code) | 22c. OFFICE SYMBOL |
|---|---|---|
| Lt. Col. Lawrence D. Hokanson | 202/767-4935 | AFOSR/NA |

DD FORM 1473, 83 APR EDITION OF 1 JAN 73 IS OBSOLETE.

Unclassified

SECURITY CLASSIFICATION OF THIS PAGE

## ABSTRACT

The present report develops electrical analogs to investigate multiple cracks on simple beams and more complex frame structures. Analog networks provide the economic tool to analyze such structures. The effect of multiple cracks on the natural frequencies of simple structures is studied in detail. It is shown that closely spaced multiple cracks are indistinguishable from an effective single crack. A severe crack on a structure can be identified if there are only minor cracks in addition to the major one. If, on the other hand, there is more than one severe crack, then the damage cannot, in general, be diagnosed with only three frequencies measurable. Nevertheless, a minimum number of cracks which are likely to be present in the structure can be established.

Characteristic equations are developed in the form of linear systems for cantilever beam and general frame structures with multiple cracks. Usefulness of relative-frequency-change curves are demonstrated and rough guidelines are provided to aid the damage diagnosis process. Several numerical examples are included which illustrate the effect of multiple cracks on frequencies.






A-1

TABLE OF CONTENTS

LIST OF FIGURES

LIST OF FIGURES (Continued)



LIST OF TABLES

# NOMENCLATURE

| Symbol | |
|---|---|
| $a$ | crack length |
| $b$ | half depth of a flexural member |
| $e$ | location of the crack on a beam with only one crack |
| $e_i (= L_i/L)$ | distance between i-1st and ith cracks on a simple beam; length of the ith beam segment in a frame structure |
| $e_{eq}$ | location of the single crack which is equivalent to a group of cracks (the definition of equivalence is given on p. 24) |
| $E$ | modulus of elasticity |
| $E_{i1}$, $E_{i2}$ | voltage sources in analog T circuit for the ith beam segment, Equation (10) (no subscript i for a one-member structure) |
| $G_i$, $G_{i0}$ | conductances in analog $\pi$ circuit for the ith beam segment, Equation (22) (no subscript i for a one-member structure) |
| $h$ | $L^2/EI\beta^2$ (subscripted when referring to the ith segment) |
| $I$ | area moment of inertia |
| $I_{i1}$, $I_{i2}$ | current sources in analog $\pi$ circuit for the ith beam segment, Eq. (23) |
| $k$ | total number of cracks on a structure |
| $k_c (k_g)$ | total number of column (girder) cracks on a frame structure |
| $L, L_0$ | length of a beam; characteristic length for a structure |
| $L_i$ | distance between i-1st and ith cracks on a simple beam; length of the ith beam segment in a structure |
| $m$ | number of spans of a frame structure |
| $\underset{\sim}{m}$ | vector of unknown moments |
| $M_i$ | resisting bending moment at the i-1st crack in a cantilever |
| $M_{i1}$, $M_{i2}$ | resisting moment at the two ends of the ith beam segment (no subscript i for a one-member structure) |
| $n_{ij}$ | defined in Equation (66) |
| $P, P'$ | variables of the analog $\pi$ circuit, Equation (20); |
| $Q, Q'$ | subscripted when referring to the ith segment |

| | |
|---|---|
| $R_j$ | relative change in jth modal frequency = $1 - \omega_j/\omega_{uj}$ |
| $R_{j_{eq}}$ | relative change in jth frequency due to an equivalent crack causing the same change in two other frequencies as the actual damage |
| S,S',T,T' | T circuit variables, Equation (7); subscripted for the ith segment |
| $\underset{\sim}{U}$ | matrix of resistances or conductances |
| $V_{i1}, V_{i2}$ | resisting cross-shear at the two ends of the ith beam segment |
| W, W' | $\pi$ circuit variables, Equation (20); subscripted for the ith segment |
| $\underset{\sim}{X}$ | coefficient matrix of $\underset{\sim}{m}$ or $\underset{\sim}{y}'$, Equations (30), (69) |
| $\underset{\sim}{X}^{(j)}$ | submatrix of $\underset{\sim}{X}$ corresponding to the jth wall of the structure |
| $y_i$ | transverse deflection at the ith crack; horizontal displacement of the ith floor |
| $y_{i1}, y_{i2}$ | transverse deflection at the two ends of the ith beam segment (no subscript i for a one-member structure) |
| $\underset{\sim}{y}$ | vector of transverse deflections |
| $y'_i$ | rotation of the ith node (prime does not imply derivative) |
| $\bar{y}'_r$ | rotation of the node r' immediately to the right of or above a crack |
| $y'_{i1}, y'_{i2}$ | rotation at the two ends of the ith beam segment |
| $Z_i, Z_{i0}$ | resistances in T circuit for the ith segment, Eq. (9) |
| $\underset{\sim}{Z}$ | coefficient matrix of $\underset{\sim}{y}$, Eqs. (30), (69) |
| $\alpha$ | defined in Equation (20) |
| $\beta$ | characteristic value; $\beta^4 = \omega^2\rho L^4/(EI)$ |
| $\beta_u$ | characteristic value of the undamaged structure |
| $\beta^{(j)}$ | jth characteristic value |
| $\beta_{eq}^{(j)}$ | jth characteristic value for the structure with an equivalent crack having two other characteristic values in common with the actual damaged structure |

| | |
|---|---|
| $\beta_{actual}^{(j)}$ | jth characteristic value for the actual damaged structure |
| $\beta_i$ | characteristic value for the ith beam segment |
| $\gamma$ | fracture damage = a/b |
| $\kappa$ | torsional spring constant of the fracture hing |
| $\nu$ | Poisson's ratio |
| $\rho$ | lineal mass density |
| $\theta_i$ | sensitivity number for the ith crack on a simple beam; sensitivity number for the crack on the ith member of a frame structure |
| $\theta_{eq}$ | sensitivity number for a crack equivalent to a group of cracks |
| $\omega_j$ | jth modal frequency |
| $\omega_{uj}$ | jth modal frequency of the undamaged structure |

## 1.0 INTRODUCTION

The study of damage diagnosis stems from the need to assess reliability of structures which have been subjected to unusual levels of excitation. Such a diagnosis problem requires the availability of an analytical model and of measurements of some structural characteristics to be used as inputs to the model. The present investigation utilizes the modal frequencies of the structure in detecting and identifying fracture damage. Damping will later be incorporated into the model.

Determination of the crack location and intensity in simple structures with only a single crack was studied in [1][1]. There it was shown that a crack can be simulated with fracture hinges representing the softening effect. The classical modal shapes for the beam elements wer assumed; the boundary conditions were imposed; and the resulting set o homogeneous equations were solved in terms of the modal frequencies. Since there are four coefficients associated with the modal shape of each beam element, the order of the resulting system is four times the number of beam elements in the structure. The approach soon loses its feasibility as the structure becomes more complicated. The present report describes another approach, namely, the use of electrical analogy in structural analysis, which greatly economizes on computation of modal frequencies of complicated frame-structures.

The introductory work on electrical analogues for solving static and dynamic problems of elastic structures is surveyed in [2]. The techniques presented there are suitable for analog computer applications. In this report, a modified and improved approach to free vibration is developed which is readily formalized and adaptable to digital programming. Electrical analogy is further developed to simulate cracks. The application of the newly developed technique is extended to investigation of the behavior of multiple cracks on structures. When the method is applied to free vibration of multi-story multi-span frame structures, natural frequencies of the analog circuit, hence modal frequencies of the frame, can

[1]Numbers in brackets denote the references.

be determined by exciting the circuit with a variable frequency excitation and by establishing the excitation frequencies at which the response is maximum. Analytically this corresponds to finding zeroes of a determinant. The order of the system for a multi-cell structure without crack is equal to the number of nodes. The order increases by two for each crack present.

## 2.0 BASIC ANALOG CIRCUITS

The mode shapes of a Bernoulli-Euler beam under transverse vibration are given by

$$y(\xi) = \bar{A}\cosh\beta\xi + \bar{B}\sinh\beta\xi + \bar{C}\cos\beta\xi + \bar{D}\sin\beta\xi \qquad (1)^2$$

where $\beta^4 = \rho\omega^2L^4/EI$; $\rho$ is the lineal density; $\omega$ is the modal frequency; L is the beam length; (EI) is the beam stiffness; and $\xi = x/L$ is the normalized axial coordinate. Four variables are associated with each end of the beam element, namely, deflection, slope (or angle of rotation), resisting moment, and shear force (Fig. 1). From Equation (1) and its appropriate derivatives at $\xi = 0$, the variables at the left end are obtained:

$$\begin{aligned} y_1 &= \bar{A} + \bar{C} \\ y_1' &= (\bar{B} + \bar{D})\beta/L \\ M_1 &= (\bar{A} - \bar{C})EI\beta^2/L^2 \\ V_1 &= (\bar{D} - \bar{B})EI\beta^3/L^3 \end{aligned} \qquad (2)$$

Equations (2) can be solved for the four coefficients in terms of the four variables

$$\begin{aligned} \bar{A} &= (y_1 + hM_1)/2 \\ \bar{B} &= (y_1' - hV_1)L/2\beta \\ \bar{C} &= (y_1 - hM_1)/2 \\ \bar{D} &= (y_1' + hV_1)L/2\beta \end{aligned} \qquad (3)$$

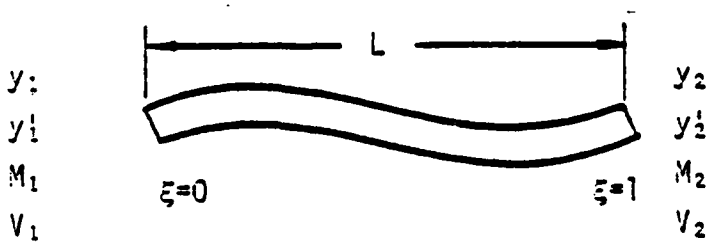


Figure 1. Beam Element under Free Vibration.

[2]Numbers in parentheses denote the equations.

where $h = L^2/EI\beta^2$. The variables at the right-end of the beam element are obtained from Equations (1) and (3) with $\xi = 1$. The result is

$$y_2 = Ay_1 + By_1'L/\beta + CM_1h - DV_1hL/\beta \tag{4a}$$

$$y_2' = Dy_1\beta/L + Ay_1' + BM_1L/EI\beta - CV_1h \tag{4b}$$

$$M_2 = Cy_1/h + Dy_1'EI\beta/L + AM_1 - BV_1L/\beta \tag{4c}$$

$$V_2 = -By_1\beta/hL - Cy_1'/h - DM_1\beta/L + AV_1 \tag{4d}$$

where

$$A = (\cosh\beta + \cos\beta)/2 \qquad B = (\sinh\beta + \sin\beta)/2$$
$$C = (\cosh\beta - \cos\beta)/2 \qquad D = (\sinh\beta - \sin\beta)/2 \tag{5}$$

Any four of the eight variables in Equations (4) can be solved for in terms of the remaining four variables. The mathematical analogy between electrical circuits and beams is based on the liner transform (4). The type and properties of the resulting circuit depend on the choice of the independent variables. In this study, angles of rotation are analogous to voltages and resisting moments are analogous to electrical currents.

## 2.1 T Circuit

When it is imposed that $\sin\beta \neq 0$, slopes and shears can be expressed in terms of resisting moments and deflections. Thus, from Equations (4)

$$\begin{Bmatrix} y_1' \\ y_2' \\ V_1 \\ V_2 \end{Bmatrix} = \frac{\beta}{2L} \begin{bmatrix} -hS & -hT & -S' & T' \\ hT & hS & -T' & S' \\ S' & -T' & S/h & T/h \\ T' & -S' & -T/h & -S/h \end{bmatrix} \begin{Bmatrix} M_1 \\ M_2 \\ y_1 \\ y_2 \end{Bmatrix} \tag{6}$$

where $h = L^2/EI\beta^2$ and

$$S = \coth\beta - \cot\beta \qquad S' = \coth\beta + \cot\beta$$
$$T = \csc\beta - \operatorname{csch}\beta \qquad T' = \csc\beta + \operatorname{csch}\beta \tag{7}$$

The first two equations in (6) can be rewritten as

$$y_1' = (Z + Z_0)M_1 - Z_0M_2 + E_1$$
$$y_2' = Z_0M_1 - (Z + Z_0)M_2 + E_2 \qquad (8)$$

where

$$Z = -(S + T)L/2EI\beta \qquad Z_0 = TL/2EI\beta \qquad (9)$$

$$E_1 = (T'y_2 - S'y_1)\beta/2L \qquad E_2 = (S'y_2 - T'y_1)\beta/2L \qquad (10)$$

Equations (8) are the Kirchhoff's equations for the active three terminal network shown in Figure 2 (T circuit)[3] with slope and moment ($y'$, $M$) being analogous to electrical voltage and current, respectively. The quantities $Z$ and $E_i$ denote resistance and voltage source, respectively. Negative resistance poses no difficulty in analytical and numerical analyses. The ends of a beam segment are simulated by the ports of the circuit. It must be observed that the electromechanical analogy described above does not simulate the differential equation of motion, but instead the solution based on the assumption of harmonic motion [2].

Boundary conditions at the ends of a beam element can be simulated as follows:

a. Free end or simply-supported end, $M = 0$: the corresponding port of the circuit to be left open (for zero current).

b. Fixed end, $y' = 0$: the corresponding port to be short-circuited (for zero voltage).

The other boundary conditions at these ends and the last two equations in (6) are utilized to express the voltage sources, Equations (10), in terms of the moments, as will be illustrated with a cantilever beam problem (Figure 3). The Kirchhoff's voltage law applied to the loop yields

$$(Z + Z_0)M_1 + E_1 = 0 \qquad (11)$$

[3]Refer to the appendix for the development of the circuit equations.

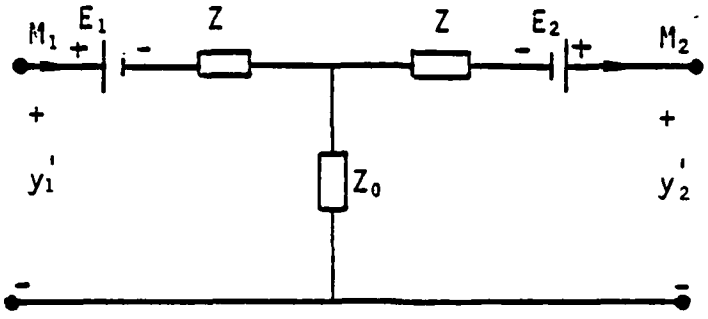


Figure 2. T-circuit Analog of a Beam under Free Vibration.

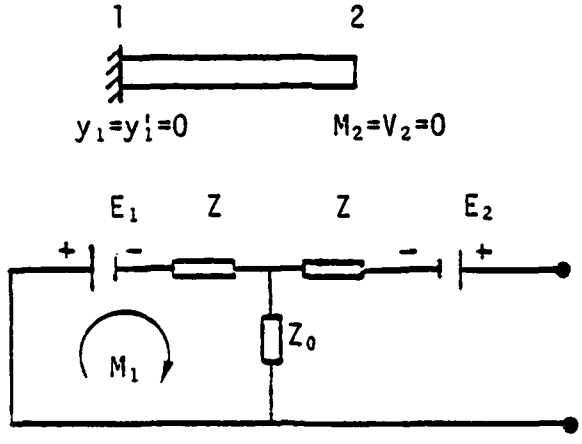


Figure 3. Cantilever Beam and its T-circuit Analog.

where Z is the analog resistance. From the last equation in (6) with $y_1 = M_2 = 0$,

$$V_2 = 0 = (T'M_1 - Sy_2/h)\beta/2L \tag{12}$$

from which

$$y_2 = hT'M_1/S \text{ and } E_1 = T'^2M_1L/2EI\beta S \tag{13}$$

The second equation in (13) is obtained from Equation (10).

Substitution of Equations (9) and (13) into (11) and the fact that $M_1 \neq 0$ result in

$$T'^2/S - S = 0 \tag{14}$$

which yields the characteristic equation of a cantilever beam, $1 + \cosh\beta \csc\beta = 0$.

In derivation of Equations (6), it is theoretically sound to impose that $\sin\beta \neq 0$. However, during the numerical search of the natural frequencies, $\sin\beta$ may get very small at some point, or the structure may actually have frequencies at or near $\sin\beta = 0$. We shall then take into consideration that $\beta$ is directly proportional to the length L of the beam element. Thereby, this problem can be solved by dividing the beam into two sections and representing each section by an individual circuit. This will be illustrated with a simply-supported beam. The beam is arbitrarily divided into two elements with a length ratio of 4/6 (Fig. 4).

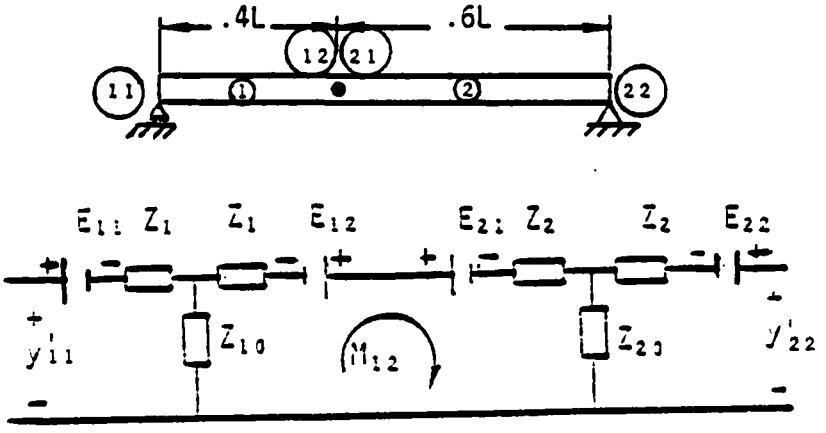


Figure 4. Simply-supported Beam Represented with Two Elements and its Analog Circuit.

With reference to the figure, the continuity conditions in slope and moment (voltage and current) at the common boundary is preserved under the cascade connection of the two basic circuits. The loop equation then yields

$$(Z_1 + Z_{10} + Z_2 + Z_{20})M_{12} - E_{12} + E_{21} = 0 \tag{15}$$

Since deflection is continuous at the interface (i.e., $y_{12} = y_{21}$), it can be shown that

$$E_{12} = S_1' y_{12}\beta_1/2L_1 \qquad E_{21} = -S_2' y_{12}\beta_2/2L_2 \tag{16}$$

where $L_1 = .4L$, $L_2 = .6L$, $\beta_1 = .4\beta$, and $\beta_2 = .6\beta$ with $\beta^4 = \rho\omega^2 L^4/EI$. From Newton's third law $V_{12} = V_{21}$, or

$$y_{12} = -hM_{12}(S_1^{\dagger} + S_2^{\dagger})/(S_1 + S_2) \tag{17}$$

Equations (9) and (15) through (17) can be combined to yield the frequency equation

$$(S_1' + S_2')^2 - (S_1 + S_2)^2 = 0 \tag{18}$$

It is to be noted that for the particular sectioning in this illustration, the same problem will arise at the fifth natural frequency where $\beta_1 = 2\pi$ and $\beta_2 = 3\pi$. Then the same procedure can be applied by further sectioning the beam. Better initial sectionings are of course possible than the one presented.

## 2.2 Π Circuit

Similar to the case of Equation (6) in the T circuit, Equation (4) can be rewritten such that resisting moments and shears are expressed in terms of deflections and slopes; that is,

$$\begin{Bmatrix} M_1 \\ M_2 \\ V_1 \\ V_2 \end{Bmatrix} = \frac{1}{h} \begin{bmatrix} QL/\beta & WL/\beta & Q' & -W' \\ -WL/\beta & -QL/\beta & -W' & Q' \\ Q' & W' & P\beta/L & -P'\beta/L \\ W' & Q' & P'\beta/L & -P\beta/L \end{bmatrix} \begin{Bmatrix} y_1' \\ y_2' \\ y_1 \\ y_2 \end{Bmatrix} \tag{19}$$

where

$$P = (\cosh\beta \sin\beta + \sinh\beta \cos\beta)/\alpha \qquad P' = (\sinh\beta + \sin\beta)/\alpha$$
$$Q = (\cosh\beta \sin\beta - \sinh\beta \cos\beta)/\alpha \qquad Q' = \sinh\beta \sin\beta/\alpha$$
$$W = (\sinh\beta - \sin\beta)/\alpha \qquad W' = (\cosh\beta - \cos\beta)/\alpha \tag{20}$$
$$\alpha = \cosh\beta \cos\beta - 1 \neq 0$$

The first two equations in (19) can be rewritten as

$$M_1 = (G + G_0)y_1' - G_0 y_2' + I_1$$
$$M_2 = G_0 y_1' - (G + G_0)y_2' + I_2 \tag{21}$$

where G and I are the analog conductance and current source, respectively, given by

$$G = (Q + W)EI\beta/L \qquad G_0 = -WEI\beta/L \tag{22}$$

$$I_1 = (Q'y_1 - W'y_2)/h \qquad I_2 = (Q'y_2 - W'y_1)/h \tag{23}$$

Equations (21) are the Kirchhoff's current equations for the active three terminal network shown in Figure 5 ($\pi$ circuit)[4] with G and I denoting a conductance and a current source, respectively. The pair (M,y') are again analogous to current and voltage. It must be noted that a $\pi$ circuit can be derived by directly inverting the system in (6). However, the resulting derivation requires more computational effort in solution of frame-structures. As an illustration, the cantilever beam of Figure 3 will now be simulated with a $\pi$ circuit. The left port of the circuit in Figure 5 is shorted yielding the circuit of Figure 6. The node voltage equation is

$$(G + G_0)y_2' - I_2 = 0 \tag{24}$$

The last equation in (19) with $y_1 = y_1' = V_2 = 0$ yields

$$y_2 = LQ'y_2'/\beta P \tag{25}$$

---

[4]Refer to the appendix for the development of the circuit equations.

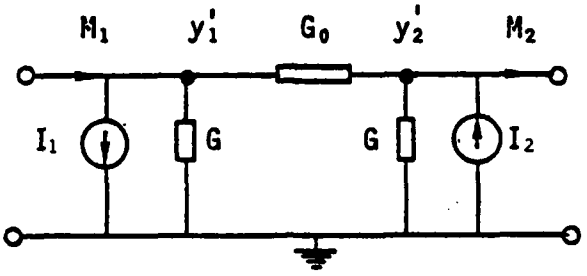


Figure 5. Π-circuit Analog of a Beam under Free Vibration.

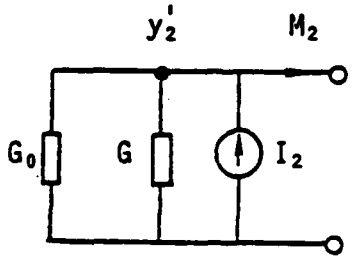


Figure 6. Analog Π-circuit for a Cantilever Beam.

The characteristic equation is obtained by substituting Equations (22, 23, 25) into (24). Namely,

$$Q - Q'^2/P = 0 \tag{26}$$

With reference to (20), Equation (26) is equivalent to $1 + \cosh\beta\cos\beta = 0$, if $1 - \cosh\beta\cos\beta \neq 0$. When the value of $\alpha$, Equation (20), approaches zero, numerical computation diverges. Similar to the approach in T circuit, the beam can be subdivided into elements as described in the previous section.

## 2.3 Simulation of Crack with Circuit Analogy

A cracked section in a beam is modeled following the method of fracture hinge [1]. The crack is mechanically represented by a torsional spring of spring constant $\kappa$. Slope is thus discontinuous at the cracked section, the discontinuity being given by $\Delta y' = M_c/\kappa$. Such a discontinuity is analogous to a voltage drop in the circuit theory. The crack can then be simulated with a resistor of resistance $-1/\kappa$. Hence, a beam with a single crack is represented by two circuits (T or $\pi$) joined by a "crack resistance," $-1/\kappa$. Examples will be given in the next chapter where it will also be shown that crack intensity is quantified by the nondimensional sensitivity number $\theta = EI/\kappa L$ [1].

## 3.0 MULTIPLE CRACKS ON SIMPLE BEAMS

In this investigation, damage diagnosis is based on the knowledge of the new modal frequencies after the damage has occurred, together with the knowledge of the material properties. If there are uncertainties about the material properties, then the frequencies must be measured prior to the damage also. This point will be explained in Section 3.2.

Each crack in a structure is characterized by two variables associated with it, namely, location (e) and intensity ($\gamma$). When these characteristic variables are known, changes in the frequencies can be computed with the method presented in this chapter. This will be called the forward problem. The inverse problem of locating and identifying the cracks, however, requires (2k + 1) measurements of frequency, where k is the number of cracks present. The extra measurement is needed to pinpoint the cracks because of the multiple-valuedness of the equations. Only in some special cases, 2k measurements are adequate to accomplish the task. On the other hand, the number k is not known a priori in a practical situation. Besides, in practice, it may not be possible to measure more than the first few modes. In application it is not possible to locate and identify the cracks deterministically when k is greater than two. However, valuable insight may be gained by investigating the forward problem.

This chapter studies the group behavior of multiple cracks on simple beams. Guidelines are presented for damage diagnosis involving multiple cracks. Examples are given to illustrate the applications of these guidelines.

A beam with k cracks can be represented by k+1 circuits joined by resistors simulating the cracks. The unknowns in the T-circuit analogy are the moments (currents) at the cracks and at the ends of the beam. Hence, there are (k+1) unknowns. On the other hand, the unknowns in the $\pi$-circuit analogy are the slopes at the ends of the beam and at the cracks. There are two unknown slopes at each crack. Hence the order of the system is larger with $\pi$ circuits. The T-circuit analog is found to

be more suitable for multiple-crack analysis. Therefore this section develops the characteristic frequency equation for the general case, establishes the conditions under which multiple cracks become equivalent to a single crack, and illustrates the inverse problem when k = 1.

## 3.1 Cantilever Beam with Multiple Cracks

Figure 7 depicts the analog circuit for a cantilever beam with k cracks. Continuity of moments at the cracked sections is preserved via the continuity of electrical currents through the "crack resistors," $-1/K_i$. The order of the system of mesh current equations is (k + 1). Namely,

$$\left.\begin{aligned}
&(Z_1 + Z_{10})M_1 - Z_{10}M_2 + E_{11} = 0 \\
&-Z_{10}M_1 + (Z_1 + Z_{10} + Z_2 + Z_{20} - 1/\kappa_1)M_2 - Z_{20}M_3 - E_{12} + E_{21} = 0 \\
&\quad\vdots \\
&-Z_{k0}M_k + (Z_k + Z_{k0} + Z_{k+1} + Z_{k+1,0} - 1/\kappa_k)M_{k+1} - E_{k2} + E_{k+1,0} = 0
\end{aligned}\right\} \quad (27)$$

From Equations (10), the analog voltage sources $\{E_{ij}\}$ are:

$$\begin{Bmatrix} E_{11} \\ E_{12} \\ E_{21} \\ \\ E_{22} \\ \cdot \\ \cdot \\ \cdot \\ E_{k2} \\ E_{k+1,1} \end{Bmatrix} = \frac{\beta}{2L} \begin{bmatrix} T_1' & 0 & \cdots & & 0 \\ S_1' & 0 & & & \\ -S_2' & T_2' & 0 & & \vdots \\ & & & & \\ -T_2' & S_2' & 0 & & \\ \cdot & & & & \\ \cdot & & & & \\ \cdot & & & & \\ 0 & \cdots & & -T_k' & S_k' \quad 0 \\ 0 & \cdots & & 0 & -S_{k+1}' \quad T_{k+1}' \end{bmatrix} \begin{Bmatrix} y_1 \\ y_2 \\ y_3 \\ \\ y_4 \\ \cdot \\ \cdot \\ \cdot \\ y_k \\ y_{k+1} \end{Bmatrix} \quad (28)$$

where $y_j$ is the deflection of the jth cracked section and $y_{k+1}$ is the deflection of the free end. These deflections are solved for by imposing

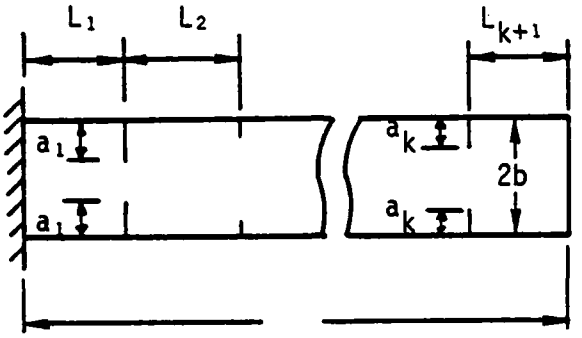


Figure 7a. Cantilever with k Symmetrical Cracks.

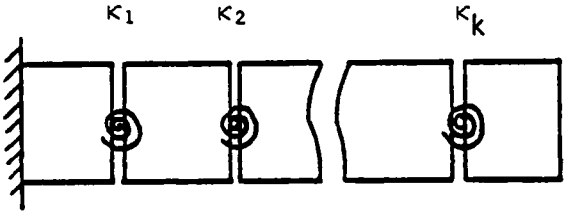


Figure 7b. Equivalent Fracture-hinge Model of the Cantilever in Figure 7a.

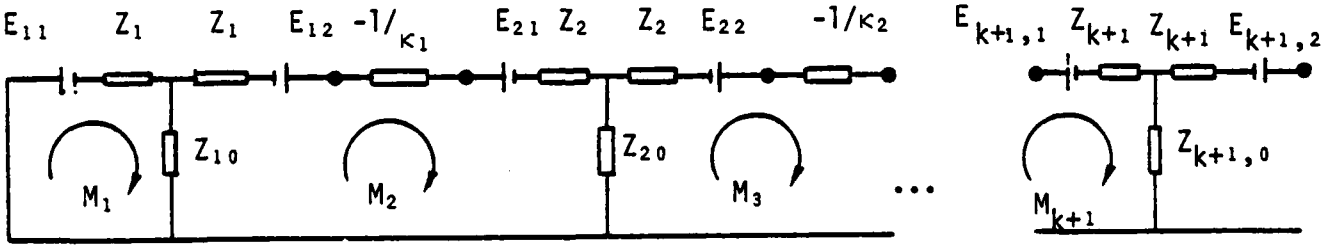


Figure 7c. T-circuit Analog for the Equivalent Model of Figure 7b.

the shear boundary and continuity conditions. That is,

$$\left.\begin{aligned} V_{i2} &= V_{i+1,1} \qquad i = 1,2,\ldots,k \\ V_{k+1,2} &= 0 \end{aligned}\right\} \tag{29}$$

where the first subscripts refer to the numbers of the elements within the beam and the second subscripts 1 and 2 denote the left and right ends of the corresponding elements. Substituting the last two equations in the T-circuit equations (6) into (29) and rearranging, we obtain

$$\frac{1}{h}\,\underset{\sim}{Z}\,\underset{\sim}{y} = \underset{\sim}{X}\,\underset{\sim}{m} \tag{30}$$

where $\underset{\sim}{y}$ and $\underset{\sim}{m}$ are vectors of deflections and mesh currents, and $\underset{\sim}{Z}$ and $\underset{\sim}{X}$ are square matrices of order k+1 given by

$$\underset{\sim}{Z} = \begin{bmatrix} S_1+S_2 & T_2 & 0 & & & 0 \\ T_2 & S_2+S_3 & T_3 & & & \cdot \\ 0 & T_3 & S_3+S_4 & T_4 & & \cdot \\ & & & & & \\ \cdot & & & & & \\ \cdot & & & & & \\ \cdot & & & & & T_{k+1} \\ 0 & \cdots & & & T_{k+1} & S_{k+1} \end{bmatrix} \tag{31}$$

$$\underset{\sim}{X} = \begin{bmatrix} T_1' & -S_1'-S_2' & T_2' & 0 & \cdots & 0 \\ 0 & T_2' & -S_2'-S_3' & T_3' & & \cdot \\ & & T_3' & -S_3'-S_4' & & \cdot \\ \cdot & & & & & T_k' \\ \cdot & & & & & -S_k'-S_{k+1}' \\ 0 & \cdot & \cdot & \cdot & \cdot & T_{k+1}' \end{bmatrix} \tag{32}$$

Hence, $\underset{\sim}{Z}$ is a tridiagonal symmetric matrix and $\underset{\sim}{X}$ is an upper triangular band matrix with a band width of 3. Solving for $\underset{\sim}{y}$ from Equation (30), provided $\underset{\sim}{Z}$ is non-singular, we have

$$\underset{\sim}{y} = h\underset{\sim}{Z}^{-1}\underset{\sim}{X}\,\underset{\sim}{m} \tag{33}$$

Substituting (33) into (28), and then the result into (27) along with the analog resistances from Equations (9)

$$(\underset{\sim}{X}^T\underset{\sim}{Z}^{-1}\underset{\sim}{X} - \underset{\sim}{U})\underset{\sim}{m} = \underset{\sim}{0} \tag{34}$$

where

$$\underset{\sim}{U} = \begin{bmatrix} S_1 & T_1 & 0 & \cdots & 0 \\ T_1 & S_1+S_2+2\theta_1\beta & T_2 & & \vdots \\ 0 & T_2 & S_2+S_3+2\theta_2\beta & & \\ \vdots & & & & T_k \\ 0 & \cdots & & T_k & S_k+S_{k+1}+2\theta_k\beta \end{bmatrix} \tag{35}$$

with $\theta_j$ being the sensitivity number for the jth crack given by [1]

$$\theta_j = EI/L\kappa_j = 3\pi(1-\nu^2)\left(\frac{b}{L}\right)\int_0^{\gamma}\lambda[f(\lambda)]^2 d\lambda \tag{36}$$

where $\gamma = a/b$ is the relative crack depth (Fig. 7a) and $f(\gamma)$ is the dimensionless fracture intensity factor for symmetric cracks [1], namely

$$f(\gamma) = (1-\gamma)^{-1.5}[1.122 - 2.363\gamma + 4.367\gamma^2 - 4.88\gamma^3 + 2.845\gamma^4 - 0.663\gamma^5] \tag{37}$$

As Equation (36) implies, $\theta_j$ is based on the total length of the beam.

For non-trivial solutions of (34), the determinant of its symmetric coefficient matrix must vanish, yielding the characteristic equation

$$\det\,(\underset{\sim}{X}^T\underset{\sim}{Z}^{-1}\underset{\sim}{X} - \underset{\sim}{U}) = 0\ . \tag{38}$$

When the crack spacings ($e_j$) and sensitivities ($\theta_j$) are known, the natural frequencies can be computed from Equation (38). In computing the matrices in Equation (38), the variables $S_i$, $T_i$, $S_i'$, $T_i'$ (Equation 7) pertaining to the ith beam segment are computed using $e_i\beta = (L_i/L)\beta$ where $\beta$ is based on the total length of the beam.

### 3.2 Damage Diagnosis with a Single Crack

Damage diagnosis using the present model is accomplished with the knowledge of frequencies after the damage has occurred. Since the characteristic equations of structures are in terms of dimensionless characteristic values $\{\beta\}$, the material properties EI and $\rho$ must be known accurately to compute $\{\beta\}$ from the measured frequencies $\{\omega\}$. If the properties are known, then $\beta$ can be computed from

$$\beta = L(\rho\omega^2/EI)^{1/4} \quad . \tag{39}$$

When three measurements of frequency are available for the case k = 1 (single crack), exact location (e) and severity ($\theta$) of the crack can be determined. The procedure will be illustrated with the cantilever beam problem developed in the previous section. The coefficient matrix in Equation (34), with k = 1, is of the form

$$\underset{\sim}{X}^T\underset{\sim}{Z}^{-1}\underset{\sim}{X} - \underset{\sim}{U} = \begin{bmatrix} h_{11} & h_{12} \\ h_{12} & h_{22} - 2\theta\beta \end{bmatrix} \equiv \underset{\sim}{H}(\beta,e,\theta) \tag{40}$$

where the $\beta$ values in Equation (40) are the post-damage values computed from Equation (39). The damage characteristics e and $\theta$ are to be determined from the determinant of $\underset{\sim}{H}$, which can be written as

$$\det[\underset{\sim}{H}(\beta,e,\theta)] = \det[\underset{\sim}{H}(\beta,e,0)] - 2\theta\beta h_{11} = 0 \tag{41}$$

where $e = L_1/L$ is the normalized crack location. It is noted that when $\beta$ assumes the pre-damage values $\{\beta_u\}$, $\det[H(\beta,e,0)]$ is equal to 0; that is, this term is the characteristic equation for the undamaged ($\theta = 0$) beam. There are three equations emerging from Equation (41) for the three known characteristic values. A numerical code for damage diagnosis

has been developed in which e is varied through the range (0,1). $\theta$ is computed, for a given e, using the first known characteristic value in Equation (41), namely,

$$\theta(e) = \det[\underset{\sim}{H}(\beta^{(1)},e,0)]/2\beta^{(1)}h_{11} \tag{42}$$

where the superscript on $\beta$ denotes which characteristic value is used. Then with the second known characteristic value, $\beta^{(2)}$,

$$\det[\underset{\sim}{H}(\beta^{(2)},e,\theta)] = 0 \tag{43}$$

where the value of $\theta$ is now substituted from Equation (42). A zero-searching routine is used to find the roots of Equation (42) which, in general, yields multiple solutions for e. $\beta^{(3)}$ can then be used to locate the crack. With e known, $\theta$ is computed from (42).

In the case when the beam deviates somewhat from the Bernoulli-Euler theory or when the material properties are uncertain, computing $\{\beta\}$ from Equation (39) may not be suitable. The knowledge of modal frequencies prior to the damage is then necessary. Since $\omega$ and $\omega_u$ are proportional to $\beta^2$ and $\beta_u^2$, respectively, where $\omega_u$ and $\beta_u$ are the values for the pre-damage structure, and $\omega$ and $\beta$ are the post-damage values, the following relation holds:

$$\beta = \beta_u(\omega/\omega_u)^{1/2} \tag{44}$$

It is assumed in (44) that the proportionality constant between $\omega_u$ and $\beta_u^2$ does not change after the damage has occurred. The characteristic equations do not involve any material properties and $\{\beta_u\}$ can be computed from the characteristic equation for the undamaged structure. With $\{\omega_u\}$ and $\{\omega\}$ measured in the field, $\{\beta\}$ can then be computed from Equation (44) and the above procedure can again be employed to determine e and $\theta$. Only the beam length L, the Poisson's ratio $\nu$, and the slenderness ratio (b/L) are required to determine the actual crack location $L_1$ and the crack depth a (Eq. 36). Since $\nu$ is nearly the same for most

metals, the theory becomes independent of the specific material of the structure if the material is a metal, if the damage is presented in terms of $L_1$ and a, and if $\{\beta\}$ are computed from Equation (44). The theory is totally independent of the material properties and dimensions if the damage is presented in terms of e and $\theta$. The data are more conveniently presented versus the relative frequencies $(\omega/\omega_u)$ or the relative frequency changes $(1 - \omega/\omega_u)$ rather than versus the absolute frequencies, whether $\{\beta\}$ are computed from Equation (39) or (44). In this investigation, relative changes are chosen as the means to convey the numerical results.

In practice, the response of structures deviate from the Bernoulli-Euler theory. It is therefore more accurate to compute $\{\beta\}$ from Equation (44). Equation (44), in effect, adjusts the parameters of the specific structure such that the structure frequencies match those predicted by the Bernoulli-Euler theory.

In practice, especially for structures whose frequencies are close to each other, the reduction in a certain frequency due to damage may be small while the reduction in the next frequency may be large enough that the post-damage value of the latter frequency may drop below that of the former. This phenomenon is called cross-over. When cross-over occurs and when one is not aware that it has occurred, the correspondence established between the pre-damage and the post-damage values of the frequencies will be in error. If, in such a case, one uses Equation (44), which involves the ratio of the pre-and post-damage values of the frequencies, the computed characteristic values will be incorrect. On the other hand, if Equation (39), which involves the structural properties, is used, a knowledge of the pre-damage frequencies is not required. Hence, it becomes immaterial which pre-damage frequency a certain measured post-damage frequency corresponds to; the important point is that there are some frequency values available which satisfy the post-damage characteristic equation (Eq. 41). If the structural properties are uncertain, they can be identified by measuring one frequency prior to the damage. That is, the constant K in the relation $\beta_u = K\omega_u^{1/2}$ can be determined by measuring one $\omega_u$ and computing the corresponding $\beta_u$ from the pre-damage characteristic equation. The same constant can later be used to

compute all the needed post-damage characteristic values $\beta$ from the measured post-damage frequencies $\omega$ by means of $\beta = K\omega^{1/2}$. In this case, however, the $R_j$ values cannot be used to present the data, since the ordering of the post-damage frequencies according to the magnitudes of their values does not correspond to the pre-damage ordering, unless the fact that cross-over has occurred is known.

## 3.3 Equivalence of Multiple Cracks to a Single Crack

### 3.3.1 Approximate Characteristic Equations

In this section, we study the conditions under which the identification of multiple cracks is not readily distinguishable from that of a single crack. For this purpose,equivalence of two cracks on a simply-supported beam to a single crack is first established analytically. Numerical results for larger numbers of cracks are then presented. It is established that, when equivalence holds, solution to the inverse problem of damage diagnosis cannot differentiate between single and multiple cracks.

Figure 8a depicts a simply-supported beam with a single crack and its T-circuit analog. The mesh current equation together with the Equations (9) and (10) yield

$$-(S_1 + S_2 + 2\theta\beta)M - (S_1' + S_2')y/h = 0 \qquad (45)$$

where M and y are the resisting moment and deflection at the cracked section, respectively. The continuity condition $V_{12} = V_{21}$ at the crack allows y to be solved for in terms of M. The characteristic equation for beam with a single crack is thus

$$(S_1' + S_2')^2/(S_1 + S_2) - (S_1 + S_2 + 2\theta\beta) = 0 \qquad (46)$$

With reference to Figure 8b, the characteristic equation for the case of two cracks is obtained in the form of Equation (38) with

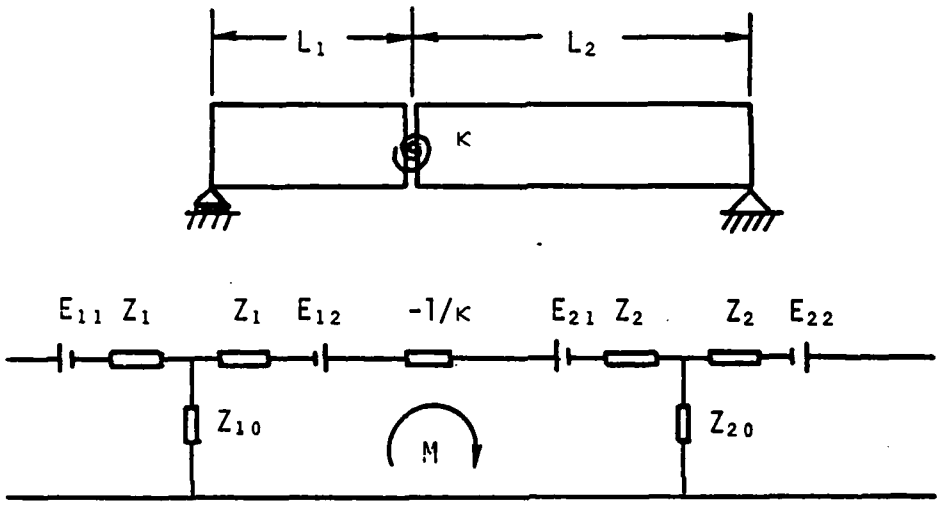


Figure 8a. Simply-supported Beam with a Single Crack and its Circuit Analog.

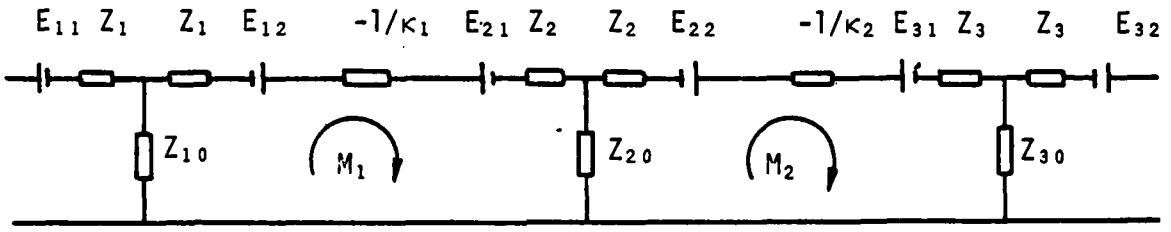


Figure 8b. Analog Circuit for a Simply-supported Beam with Two Cracks.

$$\underset{\sim}{X} = \begin{bmatrix} -S_1'-S_2' & T_2' \\ T_2' & -S_2'-S_3' \end{bmatrix} \qquad \underset{\sim}{Z} = \begin{bmatrix} S_1+S_2 & T_2 \\ T_2 & S_2+S_3 \end{bmatrix} \tag{47}$$

$$\underset{\sim}{U} = \begin{bmatrix} S_1+S_2+2\theta_1\beta & T_2 \\ T_2 & S_2+S_3+2\theta_2\beta \end{bmatrix}$$

Now, assuming that the spacing between the cracks is sufficiently small, that is, $e_2 = L_2/L = \varepsilon$; we obtain the following approximations:

$$\begin{aligned} \cosh e_{2\beta} &\doteq 1 + (\varepsilon\beta)^2/2 \quad , & \sinh e_{2\beta} &\doteq \varepsilon\beta + (\varepsilon\beta)^3/6 \\ \cos e_{2\beta} &\doteq 1 - (\varepsilon\beta)^2/2 \quad , & \sin e_{2\beta} &\doteq \varepsilon\beta - (\varepsilon\beta)^3/6 \end{aligned} \tag{48}$$

It then follows from Equations (7) that

$$S_2 \doteq 2\varepsilon\beta/3 \quad , \quad S_2' \doteq 2/\varepsilon\beta \quad , \quad T_2 = \varepsilon\beta/3 \quad , \quad T_2' \doteq 2/\varepsilon\beta \tag{49}$$

Substituting (49) into (47) and performing the necessary operations, we have, for the matrix of coefficients in (34),

$$\underset{\sim}{X}^T\underset{\sim}{Z}^{-1}\underset{\sim}{X} - \underset{\sim}{U} \doteq \frac{1}{d}\left\{\frac{4}{(\varepsilon\beta)^2}(S_1 + S_3)\begin{bmatrix} 1 & -1 \\ -1 & 1 \end{bmatrix} + \begin{bmatrix} h_{11} & h_{12} \\ h_{12} & h_{22} \end{bmatrix}\right\} \tag{50}$$

where

$$\left.\begin{aligned} d &= S_1S_3 + 2(S_1 + S_3)(\varepsilon\beta)/3 + (\varepsilon\beta)^2/3 \\ h_{11} &= 4(2 + S_1'S_3)/\varepsilon\beta + [S_1'^2S_3 + 4S_1' - S_1S_3(S_1 + 2\theta_1\beta)] \\ h_{12} &= -2(4 + S_1'S_3 + S_1S_3')/\varepsilon\beta - 2(S_1' + S_3') \\ h_{22} &= 4(2 + S_1S_3')/\varepsilon\beta + [S_1S_3'^2 + 4S_3' - S_1S_3(S_3 + 2\theta_2\beta)] \end{aligned}\right\} \tag{51}$$

The above analysis is valid at points where $S_1$, $S_1'$, $S_3$, $S_3'$ are of smaller order of magnitude than $(1/\varepsilon\beta)$. The characteristic equation for the two crack case is thus

$$\det(\underset{\sim}{X}^T\underset{\sim}{Z}^{-1}\underset{\sim}{X} - \underset{\sim}{U}) = \frac{4S_1S_3}{(\varepsilon\beta)^2}\left\{(S_1' + S_3')^2 - (S_1 + S_3)[S_1 + S_3 + 2(\theta_1 + \theta_2)\beta]\right\} + O(1/\varepsilon\beta) = 0 \qquad (52)$$

When Equations (46) and (52) are compared and it is noted that $S_1$, $S_1'$, $S_2$,$S_2'$ in Equation (46) are nearly equal to $S_1$, $S_1'$, $S_3$, $S_3'$, respectively, in Equation (52) for small values of $e_2$, it can be established that the difference between the characteristic equations for one- and two-crack cases is of the order of the product $e_2\beta$; that is, the difference is larger for higher modes. The effective sensitivity number for the two cracks approximates, as shown in (46) and (52), the sum of the individual sensitivity numbers, $\theta = \theta_1 + \theta_2$. It is shown numerically that closely spaced multiple cracks in general cannot be differentiated from a single equivalent crack.

Similar results are present for a clamped-clamped beam. In the case of a cantilever beam, however, the expressions are more complicated. Numerical results for a cantilever beam indicate the existence of an equivalent single crack to closely spaced multiple cracks. Since within 10-15% distance of the free end of a cantilever beam frequency changes are small, the numerical results are not very reliable in that region.

Equivalence of closely spaced cracks to a single crack is useful in the forward problem for studying the behavior of multiple cracks. The implication for the inverse problem of damage diagnosis is that, using the modal method, it may be impossible to distinguish between closely spaced multiple cracks and a single crack. In special cases, the equivalence exists for some configurations of multiple cracks, not necessarily closely spaced. For the general case, we may establish a lower limit on the spacing of cracks which is assumed, without loss of generality, to be uniform.

### 3.3.2 Lower Limit of Spacing

Figure 9 typically illustrates the lower limit of crack spacing for a cantilever beam when uniformly spaced multiple cracks become, as a

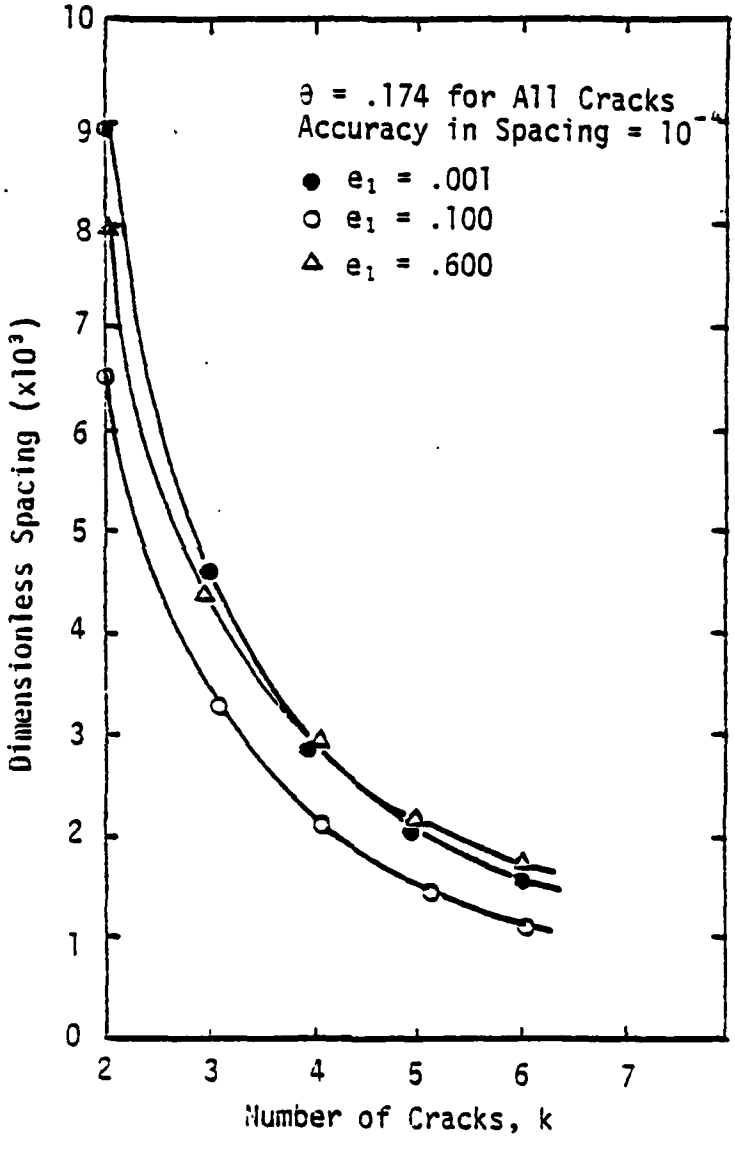


Figure 9. Lower limit of crack spacing for multiple cracks on a cantilever to be distinguishable from a single crack. (All cracks are equally spaced in each case. Agreement in the third characteristic values is ±0.001.)

whole, indistinguishable from a single crack. In Figure 9, as in subsequent illustrations, each crack assumes a sensitivity number $\theta_i$ of value 0.174 which is taken to be the lower limit for failure for a beam of slenderness ratio of 0.05 (corresponding to a relative crack depth $\gamma = a/b$ of 0.6). Figure 9 is generated by the trial method. With the number of cracks (k), individual sensitivities ($\theta_i$) and the first crack location ($e_1$) given and an initial value for the spacing between the cracks assumed, the first three characteristic values $\beta$ are computed (the forward problem). These values of $\beta$ are called the actual values. The first two of these are then used to solve for a single crack as described in section 3.2 (the inverse problem with k = 1). With the e and $\theta$ values for the equivalent single crack thus known, the third characteristic value for the equivalent crack is computed (the forward problem with k = 1). The $\beta$ values for the equivalent crack are called the equivalent characteristic values, the first two of which are the same as the actual values. If the difference between $\beta_{eq}^{(3)}$ and $\beta_{act}^{(3)}$ is not equal to the error allowance (i.e., ±0.001), then a new value for the crack spacing is assumed and the whole procedure is repeated until the required agreement is reached.

There are three cases of different crack locations in Figure 9. In the first case, the first crack is very near the built-in end, at a normalized distance of $e_1 = 0.001$ from the end. In the other two cases, the cracks are moved toward the free end with $e_1 = 0.1$ and $e_1 = 0.6$, respectively. In all the cases, (k - 1) equally spaced cracks follow the first crack. Table 1 shows the numerical data corresponding to the $e_1 = 0.1$ case. If the tolerance level in $\beta_{eq}^{(3)}$ is increased, the curves in Figure 9 will shift upward (see also Figure 12). As the number of cracks increases, they must be more closely spaced to be representable by a single crack. The lower limit of spacing depends on where the group of cracks is located. At the built-in end and at $e_1 = 0.6$, more widely spaced cracks can become indistinguishable than at $e_1 = 0.1$. The lower limit of spacing is dependent also on $\theta_i$ values. For example, when $e_1 = 0.1$, k = 2 and $\theta_1 = \theta_2 = 0.01$ (corresponding to $\gamma = 0.2$ for b/L = 0.05), the smallest crack spacing for which the double-crack damage becomes indistinguishable from a single-crack damage is $e_2 = 0.025$ under

TABLE 1

Numerical Data Corresponding to $e_1 = 0.1$ Case in Figure 9

| k | Spacing, $\varepsilon$ | $\beta^{(3)}$ | $\beta_{eq}^{(3)}$ | $\theta_{eq}$ | $e_{eq}$ |
|---|---|---|---|---|---|
| 2 | .0065 | 7.806 | 7.807 | .3479 | .1032 |
| 3 | .0033 | 7.799 | 7.800 | .5219 | .1032 |
| 4 | .0021 | 7.793 | 7.794 | .6958 | .1031 |
| 5 | .0015 | 7.789 | 7.790 | .8698 | .1029 |
| 6 | .0011 | 7.786 | 7.787 | 1.0438 | .1027 |

$\left|\beta_{eq}^{(3)} - \beta^{(3)}\right| \leq 0.001$. Figure 10 illustrates the relative changes in the first three frequencies, $R_j = 1 - \omega_j/\omega_{uj}$, corresponding to two of the cases in Figure 9 where $\omega_{uj}$ is the jth undamaged frequency. Each change is based on the corresponding ordinate in Figure 9. For any given number of cracks on a cantilever beam, the largest decrease in the fundamental frequency occurs when all the cracks are grouped at the built-in end. On the other hand, for $\theta_{eq} \geq 0.3$, the greatest change in the second frequency is observed at a location of 0.55-0.60 (Fig. 11). Such information can be utilized to set lower limits on the possible number of cracks on the structure as will be illustrated later.

Table 1 lists the equivalent locations and sensitivity numbers when cracks are grouped at $e_1 = 0.1$. The table indicates that, for the equivalent single crack,

$$\theta_{eq} \approx 0.174\ k \quad , \qquad e_{eq} \approx e_1 + \frac{\varepsilon(k-1)}{2} \tag{53}$$

where $\varepsilon$ is the uniform crack spacing. Numerical results indicate that, in general, $\theta_{eq}$ is approximately equal to the sum of individual sensitivity numbers $\theta_i$ and that the equivalent crack location $e_{eq}$ is closer to the cracks with larger sensitivity numbers.

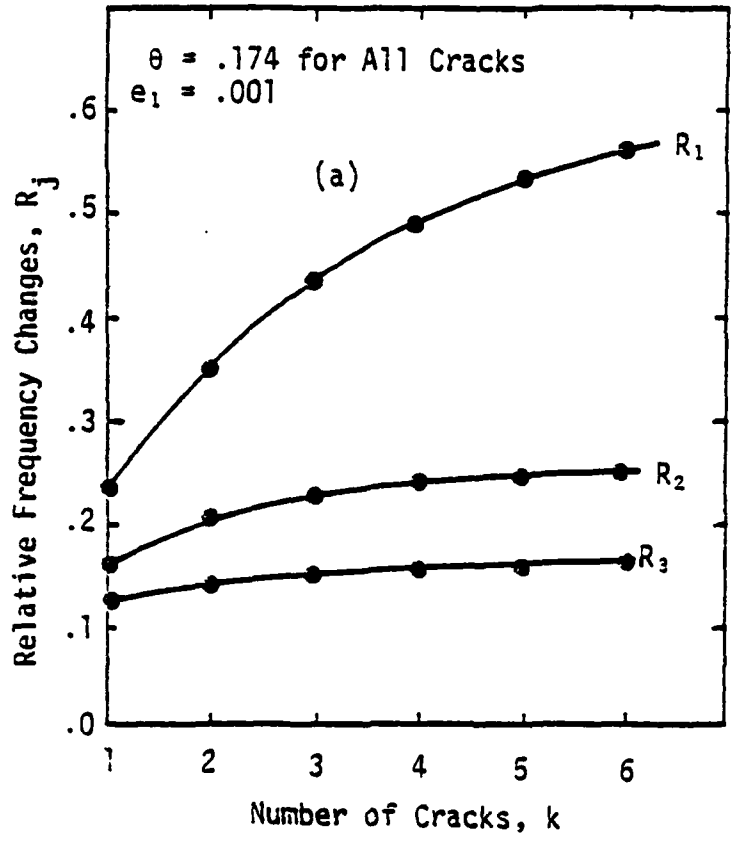


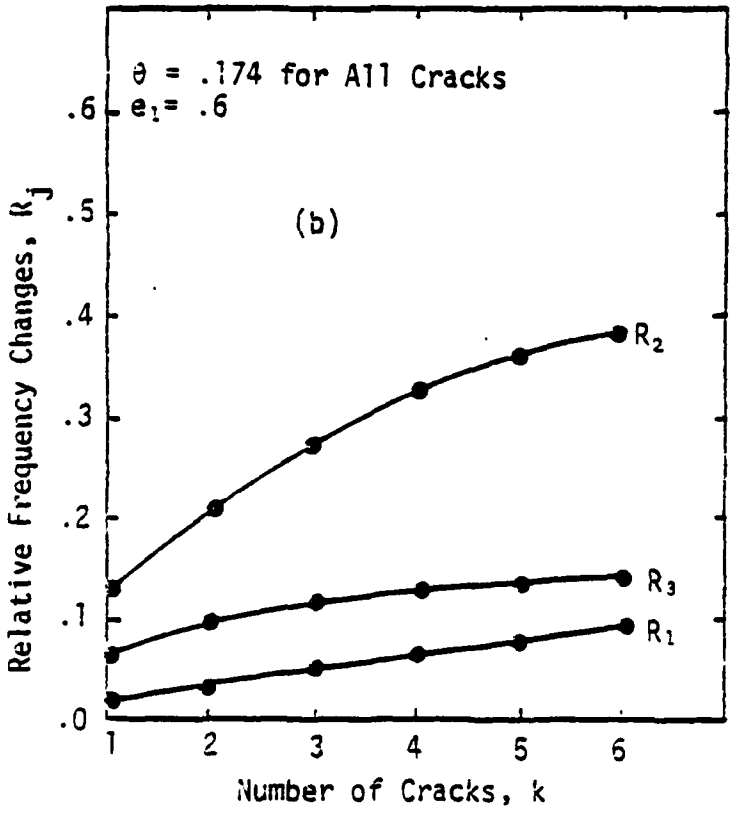


Figure 10. Relative Changes in the First Three Frequencies Corresponding to Fig. 9.

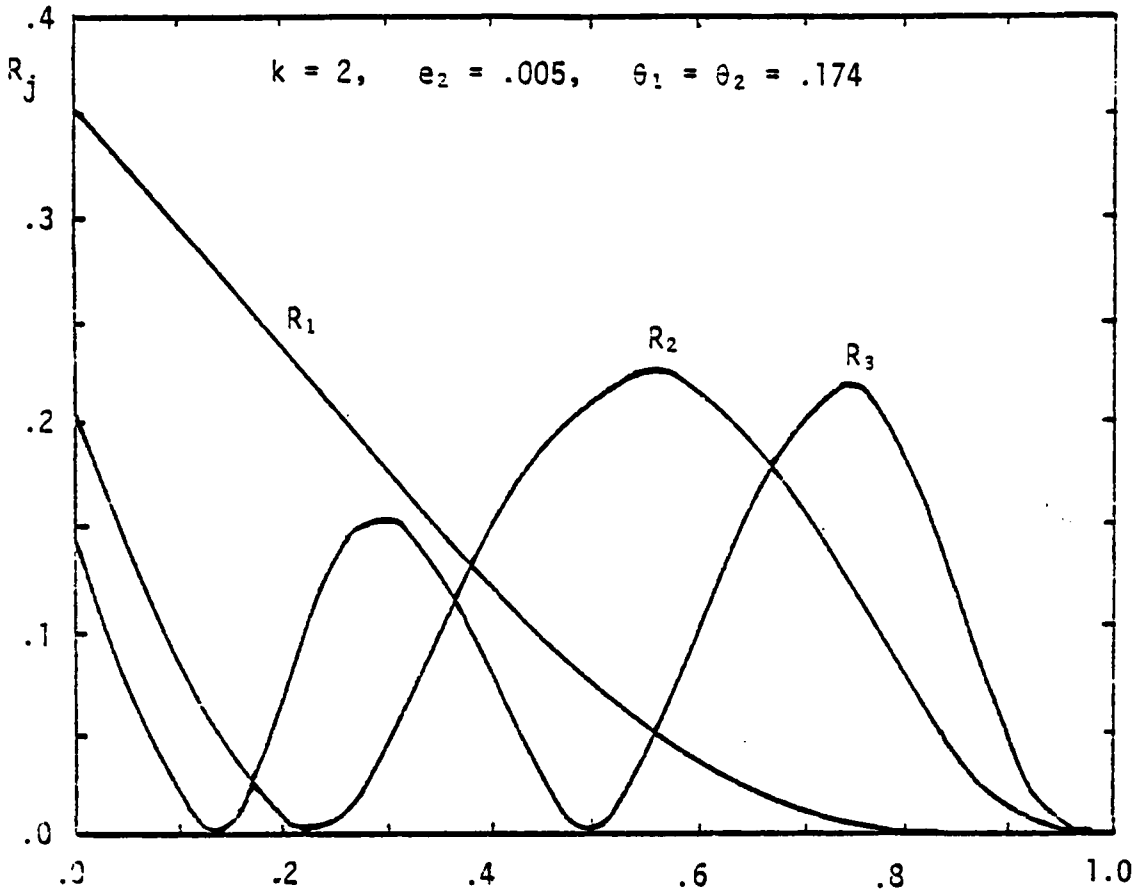


Figure 11. Relative frequency changes for a cantilever beam with two cracks as a function of the first crack location when the second crack is kept at a constant distance from the first.

### 3.3.3 Guidelines for Diagnosing Multiple Cracks

In general, with two actual characteristic values known, more than one solution exists for a single crack as was pointed out in Section 3.2. If the structure does indeed have only one crack, the crack can be diagnosed accurately with the knowledge of a third characteristic value; that is, the true solution can be pinpointed among the set of discrete solutions. In other words, two different single-crack configurations can agree in at most two characteristic values. On the other hand, a multiple-crack configuration can have the same three characteristic values as a single-crack configuration. Figure 12 compares the actual $\beta^{(3)}$ values due to two cracks on a cantilever beam with $\beta^{(3)}$ values which would stem from the presence of either of the equivalent single cracks. As in the previous illustration, equivalence is defined as $\beta_{eq}^{(j)} = \beta_{act}^{(j)}$ for j = 1,2. In Figure 12, the first crack is kept at a constant location ($e_1 = 0.1$) while the location of the second crack is varied relative to the first. In the figure, $e_2 = 0$ implies that the two cracks coincide; that is, there is one crack at $e_1 = 0.1$ of $\theta = 0.174 + 0.174 = 0.348$. $\{\beta_{act}^{(j)}, j = 1,2,3\}$ is computed first for each $e_2$ value (the forward problem with k = 2). The first two $\beta_{act}$ values are then used to solve for the equivalent single cracks (i.e., to solve for $e_{eq}$ and $\theta_{eq}$. $\beta_{eq}^{(3)}$ is then computed corresponding to each $(e,\theta)_{eq}$. There are two single-crack solutions for each $\{\beta_{act}^{(j)}\}$ set shown by the $\beta_{eq_1}^{(3)}$ and $\beta_{eq_2}^{(3)}$ curves in Figure 12. The second solution will be ignored since $\beta_{eq_2}^{(3)}$ is significantly different from $\beta_{act}^{(3)}$ over most of the range of $e_2$. For small values of $e_2$, the actual and equivalent $\beta^{(3)}$ values agree closely. In such a case, the location of the damage can be established accurately ($e_{eq}$), although the number and intensity of the cracks are uncertain. (In a real situation only $\{\beta_{act}^{(j)}\}$ and $\{\beta_{eq}^{(j)}, e_{eq}, \theta_{eq}\}$ are known, the former from the measured $\{w_j\}$ and the latter by computation.) As the spacing between the cracks, $e_2$, increases, $\beta_{eq_1}^{(3)}$ deviates more from the actual value and $e_{eq}$ is no longer indicative of the damage location. The only conclusion that can be drawn in this case is that there is more than one major crack on the beam.

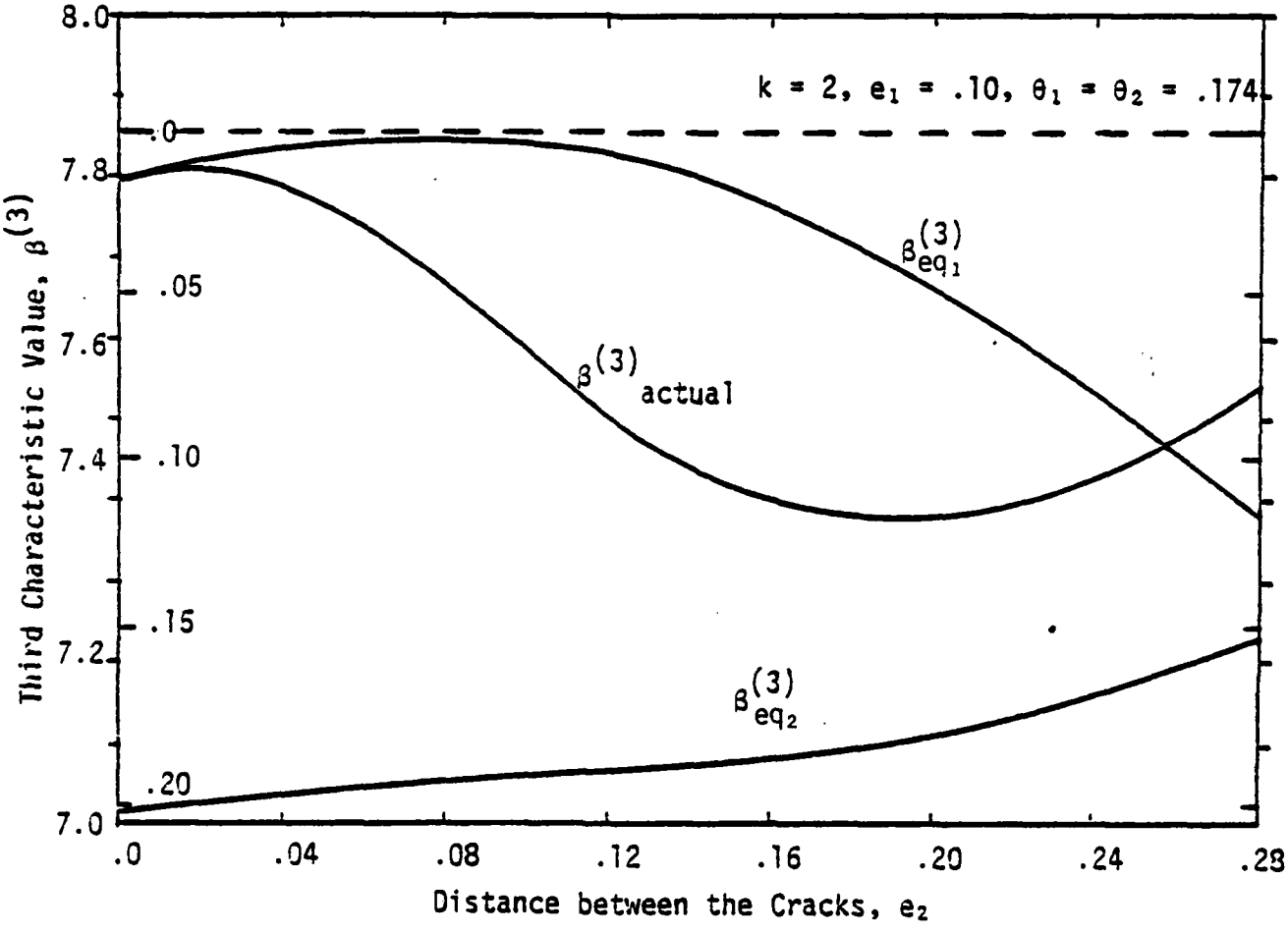


Figure 12. Third characteristic value ($\beta^{(3)}_{act}$) variation as a function of the location of the second crack with the first crack fixed. The other curves represent $(\beta)^{(3)}$ values yielded by the single cracks -solved using the first two actual modes.

Variations of the location and intensity of the equivalent crack giving rise to $\beta^{(3)}_{eq_1}$ are plotted in Figure 13. For small values of $e_2$, $\theta_{eq_1} \simeq \theta_1 + \theta_2$ and $e_{eq_1} \simeq e_1 + e_2/2$. The two upper curves in Figure 12 intersect a second time at $e_2 \simeq 0.255$. This means the following: two cracks, one at $e_1 = 0.1$, the other at a normalized distance of 0.255 away from it with $\theta_1 = \theta_2 = 0.174$ cause the same decrease in the first three frequencies as a single crack located at $e_1 = 0.024$ with $\theta = 0.187$ (from Fig. 13). Furthermore, there may be other combinations of multiple cracks which may cause the same frequency changes. It is clear that probabilistic methods must be resorted to in diagnosis of multiple cracks when an insufficient number of frequency measurements are available. Nevertheless, some qualitative conclusions may be reached with the help of Figures 9-11 which are independent of material properties. In particular, when a solution has been obtained for a single crack and a decision has to be made between a single crack and a group of closely-spaced less severe cracks, one may argue that formation of a single crack is more likely for a beam undergoing bending. In other words, a small mode I type crack is likely to propagate under bending rather than other cracks forming nearby. On the other hand, one severe and several minor cracks may exist distributed along a structure in which case the objective is to be able to diagnose the major crack. Guidelines may be established qualitatively based on the frequency change curves for a cantilever beam, Figure 11, in which case we may propose that

a. If $R_1$ is considerably smaller than $R_2$ and/or $R_3$, then the (major) crack(s) is at a normalized distance greater than ~0.45 from the built-in end (Fig. 11). In addition,

i. if $R_2$ is considerably larger than $R_3$, the crack is located around 0.45-0.65 relative to the built-in end (Fig. 10b)(see Example 3 below);

ii. if $R_3$ is larger than $R_2$, the crack is at a distance greater than ~0.7 or;

iii. if $R_2$ and $R_3$ are comparable, then there may be one major crack at 0.65-0.70, or two major cracks, one each in the peak regions of the $R_2$ and $R_3$ curves.

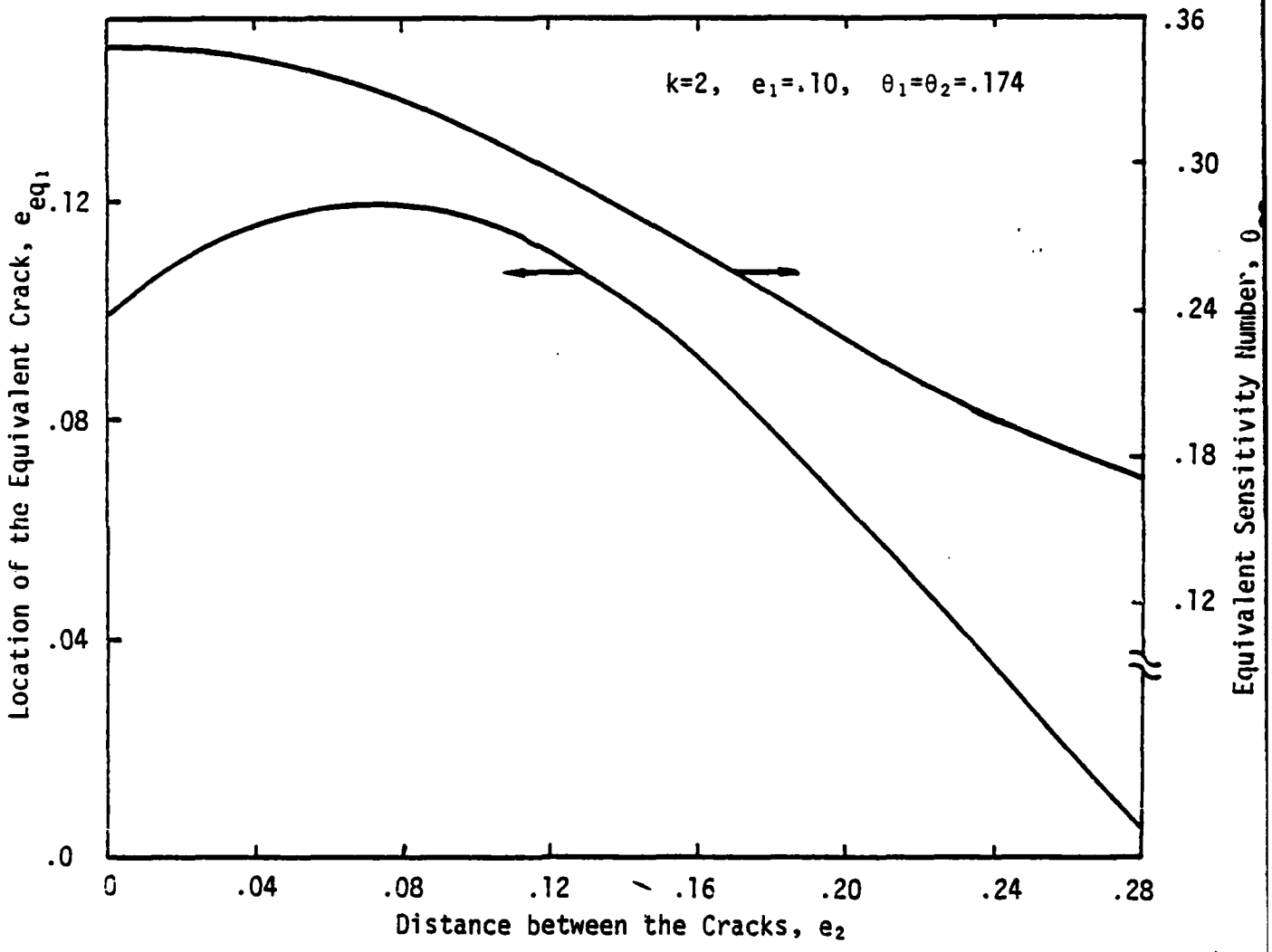


Figure 13. Location and Intensity of the First Equivalent Crack Corresponding to $\beta^{(3)}_{eq_1}$ in Fig. 12.

b. If $R_2$ is significantly smaller than both $R_1$ and $R_3$, the crack is in the region 0.2-0.3, or there may be a (major) crack at 0.2-0.3 and another (major) one at a distance greater than 0.8, the latter being more likely if $R_3$ is greater than $R_1$.

c. If $R_1$ is significantly larger than both $R_2$ and $R_3$, and $R_2$ and $R_3$ are rather small, the crack is at 0.1-0.2.

d. If the values of $R_1$, $R_2$ and $R_3$ are comparable, several possibilities exist. To list a few, there may be a number of cracks distributed over the beam (Examples 1 and 4 below); the crack may be at 0.35-0.40; or there may be a crack at 0.0-0.3 and a few others at locations greater than ~0.5.

The term "major crack" employed in the present report stems from the assumption that a beam fails if an individual crack reaches a relative depth of 0.6. Whether a shallower crack may be considered major depends on the particular application. The following table presents $\theta L/b$ values corresponding to a range of relative crack depths $\gamma$. $\nu$ is taken to be 0.3. Thus, if $\gamma = 0.3$ is considered serious for a beam of $b/L = 0.05$, then a crack with $\theta$ greater than 0.024 would signal a major crack.

| $\gamma$ | $\theta L/b$ |
|---|---|
| .1 | .051 |
| .2 | .204 |
| .3 | .484 |
| .4 | .966 |
| .5 | 1.825 |
| .6 | 3.485 |

In the present study, only the first three natural frequencies are assumed measurable. The peak locations of $R_2$ and $R_3$ curves in Figure 11 are weak functions of $\theta$ and shift to the right as $\theta$ increases. For example, as $\theta$ is increased from 0.01 to 0.50 (effective value for a few closely spaced cracks), the peak of the $R_2$ curve shifts from the location 0.530 to 0.563, while the second peak of the $R_3$ curve shifts from 0.710 to 0.760. (See also [1], pp. 29-31.)

Similar guidelines for different structures can be established based on minimum and maximum frequency changes although the procedure may become tedious for more complicated structures. The following examples illustrate some of the applications. In all the examples, a slenderness ratio of b/L = 0.05 is assumed.

Example 1. To illustrate the uncertainties involved in damage diagnosis when the three $R_j$ values are comparable in value, the following relative frequency changes are assumed to have been computed from the measured frequencies of a cantilever beam: $R_1 = .0579$, $R_2 = .0586$, $R_3 = .0591$. It is to be determined whether the damage mainly consists of one major crack.

The (actual) characteristic values are computed from

$$\beta_{act}^{(j)} = \beta_u^{(j)}(1 - R_j)^{1/2} \tag{54}$$

where $\{\beta_u^{(j)}\}$ are the undamaged characteristic values. The first three of these for a cantilever are 1.8751, 4.6941, and 7.8548. From Equation (54) in particular, $\beta_{act}^{(3)} = 7.6192$. The first two actual characteristic characteristic values yield, according to the procedure given in Section 3.2, one solution for a single crack located at $e_{eq} = .372$ with $\theta_{eq} = .128$ (corresponding to a relative crack depth of $\gamma = .55$). These equivalent values are then used in the forward problem with $k = 1$ (Equations 31, 32, 35, 38) to determine the third characteristic value due to the equivalent crack. The computation thus yields $\beta_{eq}^{(3)} = 7.614$. Then,

$$\beta_{act}^{(3)} - \beta_{eq}^{(3)} = .0018 \quad .$$

If we assume, for the sake of argument, that $\beta_{eq}^{(3)}$ is much more accurate $\beta_{act}^{(3)}$ and if the accuracy in $\beta_{act}^{(3)}$ is not better than ±.0018, the equivalent single crack solution may be accepted as the true damage diagnosis. On the other hand, the given $R_j$ data were actually generated in a

forward problem with ten cracks of equal intensity ($\theta$ was taken to be .01 [i.e., $\gamma$ = .2] for all the cracks) located such that $e_1$ = .001, $e_i$ = .094 for i = 2,3,...,10. Thus, in this case, even though the actual and equivalent $\beta^{(3)}$ values match closely, a firm diagnosis cannot be reached.

Example 2. The frequency changes and the third characteristic value have been computed from the measured frequencies similar to the first example: $R_1$ = .379, $R_2$ = .210, $R_3$ = .144, $\beta^{(3)}_{act}$ = 7.2672. What conclusions on the damage configuration can be reached from these?

The first two characteristic values, computed as in the first example, yield two solutions for an equivalent single crack. One of the solutions yields a $\beta^{(3)}_{eq}$ value which is much different from $\beta^{(3)}_{act}$ and is therefore disregarded. The solution which gives $\beta^{(3)}$ = 7.2678 is $e_{eq}$ = .0077 and $\theta_{eq}$ .400. The largest value of $R_1$ for any number of $\theta_{eq}$ = .400. The largest value of $R_1$ for any number of cracks occurs when all the cracks are grouped at the built-in end (Fig. 11). From Fig. 10a, when there are two closely-spaced cracks at the built-in end with $\theta_1 = \theta_2$ = .174, $R_1$ is equal to 0.354. For three cracks in the same region, $R_1$ = .432. The measured value of $R_1$ given above is .379. Hence, it can be concluded that there are at least three cracks on the beam (based on the assumption that $\theta$ for each crack is not greater than the limit of failure, 0.174, for b/L = .05). In principle, a large number of minor cracks (i.e., cracks with $\theta$ less than 0.01 in this case) can cause the same reduction in the first three frequencies as given in the problem statement. However, it may be argued that the likelihood of having several major cracks distributed in the peak regions of the $R_j$ curves is greater.

Example 3. This example illustrates the effect of minor cracks on $R_j$ values when minor cracks are present in addition to a major crack on a cantilever beam. The locations and intensities of the cracks are known. The characteristic values $\beta^{(j)}$ are determined from Equation (38) in Section 3.1 (the forward problem). The relative frequency changes are then determined from the characteristic values, namely,

$$R_j = 1 - \left( \frac{\beta^{(j)}}{\beta_u^{(j)}} \right)^2 . \qquad (55)$$

a. First the analysis will start with one crack (Fig. 14a), i.e., $k = 1$, at $e = .54$ (in the peak region of the $R_2$ curve, Figure 11) with $\theta = .174$ ($\gamma = .6$). The relative frequency changes are then computed as $R_1 = .029$, $R_2 = .137$, $R_3 = .014$.

b. Now, in addition to the crack in part (a), there are five more cracks of intensity $\theta = .0026$ ($\gamma = .1$) each, distributed on the cantilever such that $e_1 = e_2 = e_3 = e_5 = .1$, $e_4 = .24$, and $e_6 = .09$ (Fig. 14b). The actual characteristic values are computed as $\beta^{(1)} = 1.840$, $\beta^{(2)} = 4.351$, and $\beta^{(3)} = 7.768$ from which $R_1 = .037$, $R_2 = .141$, $R_3 = .022$. If these values of $R_j$ were computed from actual measured frequencies and the damage were to be diagnosed (the inverse problem), then $\{\beta^{(j)}\}$ would be computed from Equation (54) in Example 1. When this is the case, $\beta^{(1)}$ and $\beta^{(2)}$ are used to find a solution for a single crack which is $(e_{eq}, \theta_{eq}) = (.51, .183)$. This single crack would produce $\beta_{eq}^{(3)} = 7.845$ or $R_{3eq} = .0024$.

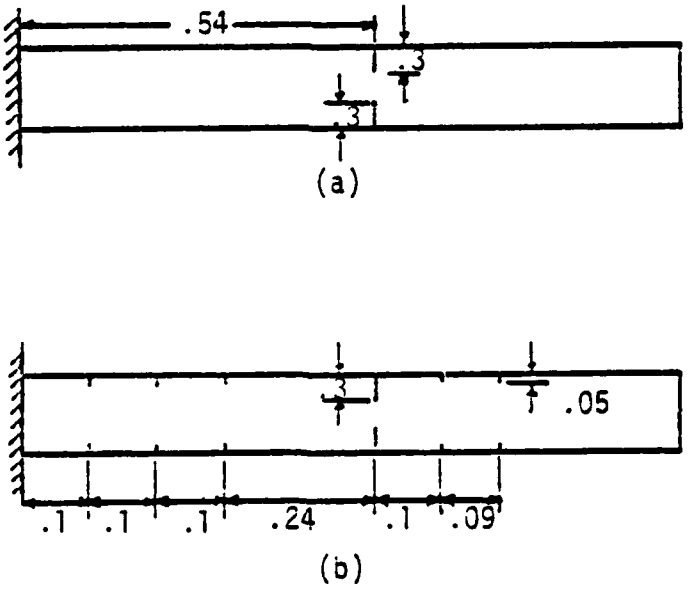


Figure 14. Cantilever with One and Six Cracks (distances are normalized based on the beam dimension in the corresponding direction).

c. The same case as in (b) except $\theta_i$ are changed to .01 ($\gamma$ = .2) with the major crack remaining the same, i.e., $\theta_4$ = .174. Hence, the depths of the minor cracks are doubled. The values of $e_i$ and $\theta_i$ are used, as in the previous cases, in the forward problem to compute $R_1$ = .058, $R_2$ = .151, $R_3$ = .043. $R_1$ and $R_2$ are in turn used in the inverse problem of damage diagnosis with k = 1 to obtain $(e_{eq}, \theta_{eq})$ = (.47, .224), $\beta_{eq}^{(3)}$ = 7.830, $R_{3_{eq}}$ = .0064.

The above cases indicate that the value of $R_2$ did not change significantly when minor cracks were added to the beam. If this were an actual damage diagnosis problem, in which case only $\{\beta^{(j)}\}$ and $\{R_j\}$ would be known from the measured data, then a decision would have to be made about the computed $(e_{eq}, \theta_{eq})$. In case (b), $R_3$ = .022 whereas $R_{3_{eq}}$ = .0024. In case (c), $R_3$ = .043, but $R_{3_{eq}}$ = .0064. Hence, based only on comparison of $R_{3_{eq}}$ with the actual values of $R_3$, the solutions for $(e_{eq}, \theta_{eq})$ would be rejected. Nevertheless, the equivalent damage parameters in both cases closely identify the major crack located at the distance of .54 from the built-in end with $\theta$ = .174. When there is no minor crack on the beam, as in case (a), $(e_{eq}, \theta_{eq})$ would be computed as (.54, .174). The effect of the minor cracks on $(e_{eq}, \theta_{eq})$ is thus seen to be small. Hence, it is concluded that, when the given $R_j$ values exhibit a pattern such as in this example, the discrepancy in $R_3$ and $R_{3eq}$ or in $\beta_{act}^{(3)}$ and $\beta_{eq}^{(3)}$ can be ignored when the interest is in diagnosing the major crack.

Example 4. This example illustrates different crack configurations which cause the same decreases in the first three frequencies. In each case, the crack locations and intensities are given from which the characteristic values and the relative frequency changes are computed (the forward problem).

The three crack configurations are

a. $k = 3$, $e_1 = 0.013$, $e_2 = 0.404$, $e_3 = 0.408$
$\theta_1 = \theta_2 = \theta_3 = 0.05$ ($\gamma = 0.405$);

b. $k = 4$, $e_1 = 0.001$, $e_2 = 0.15$, $e_3 = 0.23$, $e_4 = 0.25$
$\theta_1 = \theta_2 = \theta_4 = 0.01$ ($\gamma = 0.2$), $\theta_3 = 0.174$ ($\gamma = 0.6$);

c. $k = 8$, $e_1 = 0.001$, $e_2 = 0.06$, $e_3 = 0.14$, $e_4 = 0.20$,
$e_5 = e_6 = e_7 = 0.10$, $e_8 = 0.19$
$\theta^i = 0.021$ ($\gamma = 0.28$) for all 8 cracks.

All yield the same changes in the first three natural frequencies, namely,

$$R_1 = 0.099, \quad R_2 = 0.108, \quad R_3 = 0.089.$$

There may likely be other combinations of cracks which produce the same results. When the first two characteristic values are used to solve for a single crack (the inverse problem of damage diagnosis), $e_{eq} = 0.384$, $\theta_{eq} = 0.249$, $R_{3_{eq}} = 0.081$ are obtained. If the above $R_j$ values had been the actual measured values for a damaged cantilever and if the true situation had been as in (b), then the major crack ($\theta_3 = .174$), which is at a distance of 0.381 from the built-in end, would have been diagnosed accurately. However, uncertainties always exist when the three $R_j$ values are comparable to each other as illustrated in this example.

Example 5. This example is intended to show that, when multiple cracks exist on a beam, a crack which is located in the peak region of an $R_j$ curve affects the corresponding frequency, $w_j$, the most.

a. Given $k = 1$, $e_1 = 0.001$, $\theta_1 = 0.174$. The frequency changes are computed as (the forward problem)

$$R_1 = 0.234, \quad R_2 = 0.162, \quad R_3 = 0.125.$$

b. A second crack is added to case (a) such that $e_2 = 0.546$ (i.e., near the peak region of the $R_2$ curve, Figure 11) and $\theta_2 = 0.174$. Then

$$R_1 = 0.246, \quad R_2 = 0.272, \quad R_3 = 0.162.$$

c. A third crack is added to case (b) such that $e_3 = 0.185$ (i.e., near a peak region of the $R_3$ curve) and $\theta_3 = 0.174$ [parameter values in cases (a-b) are preserved]. Then

$$R_1 = 0.247 \quad R_2 = 0.301, \quad R_3 = 0.250.$$

If $\theta_3 = 0.01$ instead of 0.174, then

$$R_1 = 0.246, \quad R_2 = 0.273, \quad R_3 = 0.167.$$

In case (b), the greatest dcrease relative to case (a) occurred in the second frequency, whereas in case (c) it was the third frequency that suffered the largest decrease relative to case (b) although this decrease was insignificant for $\theta_3 = 0.01$. The example illustrates the effect of crack location and intensity on the frequencies and confirms the usefulness of curves such as Figure 11 to diagnosis of damage as outlined in the guidelines presented earlier.

Example 6. In all the above examples, $\beta^{(1)}$ and $\beta^{(2)}$ have been used in the inverse problem of diagnosing the major crack as described in Section 3.2. It has been found numerically that using the pair ($\beta^{(1)}$, $\beta^{(3)}$ (or ($\beta^{(2)}$, $\beta^{(3)}$) yields better results in some cases as this example illustrates.

a. Given $k = 4$, $e_1 = 0.001$, $e_2 = e_3 = 0.15$, $e_4 = 0.33$,
$\theta_1 = \theta_2 = \theta_3 = 0.01$, $\theta_4 = 0.174$

which result in

$$R_1 = 0.049, \quad R_2 = 0.137, \quad R_3 = 0.119$$

b. If it is now assumed that the above $R_j$ values have been obtained from the measured frequencies and if $\{\beta^{(j)}\}$ are computed from Equation (54), then $\beta^{(1)}$ and $\beta^{(2)}$ can be used in the inverse problem to solve for the single crack

$$e_{eq} = 0.475, \quad \theta_{eq} = 0.193, \quad R_{3_{eq}} = 0.004.$$

If, instead, $\beta^{(2)}$ and $\beta^{(3)}$, which correspond to the largest two of the three $R_j$ values, are used, the diagnosis yields two possible solutions, namely,

$$e_{eq} = 0.372, \quad \theta_{eq} = 0.422, \quad R_{1eq} = 0.161$$

and

$$e_{eq} = 0.647, \quad \theta_{eq} = 0.217, \quad R_{1eq} = 0.015$$

The second one of the last two solutions is more likely since $R_{1eq} = 0.015$ is closer to the measured value of $R_{1act} = 0.049$. Indeed, the location diagnosed, $e_{eq} = 0.647$, is close to the location of the major crack which is at the distance of 0.631 from the built-in end.

Other examples can be given wherein a certain pair of $\beta^{(j)}$ values yields better diagnosis. However, it is not clear at this point which pair to choose in each case.

It should be noted that the sensitivity number $\theta$ is a measure of how sensitive the natural frequencies are to given crack depth and location as a function of the slenderness ratio. Decrease in natural frequencies is greater for larger values of $\theta$. Between two cracked beams with the same crack location and relative crack depth, $\theta$ for the more slender one will be smaller giving rise to smaller $R_j$ values. For example, for $\gamma = 0.6$ (and $\nu = 0.3$), $\theta = 0.0697$ when $b/L = 0.02$ and $\theta = 0.0174$ when $b/L = 0.005$. Thus, in practice it is relatively harder to diagnose damage in slender beams.

## 4.0 General Two-Dimensional Frame Structure

This chapter expounds a generic model of a two-dimensional multi-storied frame (Fig. 15) with n stories and m spans (thus m + 1 anchors). A formalized scheme is developed for obtaining the modal frequencies of such a structure with or without cracks. In the T-circuit analogy, the characteristic equation for the structure is developed through the mesh current (moment) equations. Hence, the unknowns are the moments at the frame joints and at the cracks. There are (p - 1) unknown moments at a frame node where p beams join together. Because the moment is continuous across a crack, there is one unknown moment for each crack. It follows that the order of the resulting linear system, which is equal to the number of unknowns, is [n(3m + 1) + k] for a frame with k cracks. On the other hand, in the $\pi$-circuit analogy, node voltage (slope) equations lead to the characteristic equation. Slope is continuous at a frame joint; therefore, there is one unknown slope for each frame joint regardless of the number of beams connected there. However, there are two unknown slopes at each crack location, one on each side of the crack. In other words, slope is discontinuous across a crack. The structure is assumed rigidly fixed at the ground level; hence, the slopes are zero at the anchors. The order of the system is thus [n(m + 1) + 2k] with $\pi$ circuits. The $\pi$-circuit analogy is therefore preferred over the T-circuit analogy, since the order of the system for $k < 2mn$ is smaller in the former.

The procedure to obtain the characteristic equation of the frame structure can be outlined as follows:

1. $\pi$ circuits simulating individual columns and girders joining at right angles are interconnected such that the boundary conditions (Ref. 1, p. 40) at the analog-frame joints are observed. (It will be shown that a network diagram need not actually be drawn.)

2. For each crack present on any element, one more $\pi$ circuit (hence, two more unknown slopes-voltages) and one crack resistance (Section 2.3) are added to the network. A girder or a column with p cracks is thus simulated with (p + 1) $\pi$ circuits connected in cascade via the

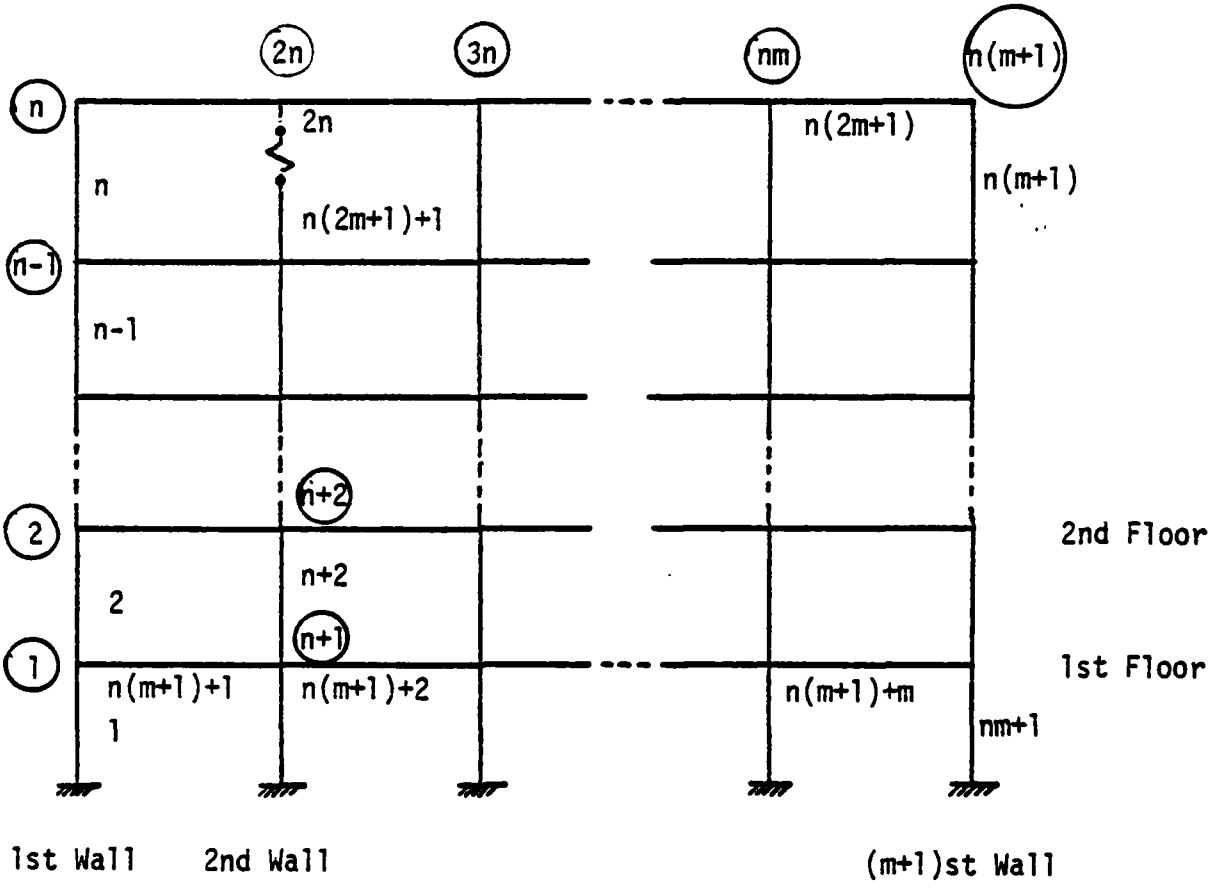


Figure 15. General n-story m-span Frame Structure.

crack resistances. The first and the (p + 1)th circuits are then connected with the rest of the network according to Step 1.

3. Kirchhoff's current law is written in terms of the node voltages which correspond to the angles of rotation at the frame joints and at the cracks.

4. Under free vibration, the coefficient matrix obtained in Step 3 must be singular. If the damage parameters (i.e., location and severity) for each crack are known, the characteristic values of the structure, $\{\beta\}$, can be determined from the zero determinant of the coefficient matrix (the forward problem). If the characteristic values are known and a diagnosis of the damage is required (the inverse problem), the method in Secton 3.2 is used to find a solution for a single crack, similar to the examples in the previous chapter.

The approach taken here results in a formal scheme which can be applied to frame structures without referring to an actual network diagram. Reference will be made to Figure 5. The word "wall" will denote the union of all the columns on the same vertical line. Each node and each beam element is identified by a number. Numbers corresponding to the nodes are encircled in the figure. The numbering order for the beam elements begins at the left lowest column, proceeds up through the columns on the first wall, returns back to the second anchor, proceeds up vertically, and continues in that order. Once the columns are finished, girders on each floor are numbered progressively from left to right starting with the first floor and continuing on with the upper floors. Quantities related to a beam element such as G, P, Q, etc. are subscripted by the number of the element. Each node is numbered by the column under the node. If there are $\ell$ cracks on a column (girder), the original number of the beam element refers to the uppermost (rightmost) segment of the column (girder) which is now represented by $\ell + 1$ beam segments. The other segments are numbered following the largest number in the scheme. Due to discontinuity of slope at a crack, two new nodes are created on the two sides of each crack.

## 4.1 Analog Circuit Equations and Boundary Conditions

### Nodal Equations:

Figure 16a shows a typical node r at the intersection of column elements r, s and girder elements p, q. In reference to Figures 5 and 16a, the sum of the branch currents entering the node r are set equal to zero. Namely,

$$(y'_i - y'_r)G_{po} + (y'_j - y'_r)G_{qo} + (y'_k - y'_r)G_{ro} + (y'_\ell - y'_r)G_{so} \qquad (56)$$
$$- y'_r(G_p + G_q + G_r + G_s) + I_{p2} - I_{q1} + I_{r2} - I_{s1} = 0$$

where $(y'_i - y'_r)$ is the analog voltage difference between the nodes i and r and $G_{po}$ is the conductance which connects these two nodes. The current sources appearing in Equation 56 are dependent on the transverse deflections of the two ends of the beam elements to which they correspond. Under small deformation theory, vertical deflection of the nodes shown in Figure 15 is, by second order approximation, equal to zero. Thus, in Figure 16a $y_{p2} = y_{q1} = 0$, $y_{p2}$ and $y_{q1}$ denoting the deflections of the right end of the pth girder and left end of the qth girder, respectively. If, in addition, the nodes i and j do not bound cracks, then $y_{p1} = y_{q2} = 0$. Consequently, $I_{p1} = I_{p2} = I_{q1} = I_{q2} = 0$ from Equation (23). On the other hand, $I_{r2}$, for instance, is not zero since, in general, $y_{r1} \neq 0$ and $y_{r2} = y_{s1} \neq 0$ (i.e., side sway is allowed).

Upon substitution of Equation (22) into (56),

$$-y'_r(n_{p1}Q_p + n_{q1}Q_q + n_{r1}Q_r + n_{s1}Q_s) - y'_i n_{p1}W_p - y'_j n_{q1}W_q - y'_k n_{r1}W_r$$
$$-y'_\ell n_{s1}W_s + \left(\frac{L}{EI\beta}\right)_0 (I_{p2} - I_{q1} + I_{r2} - I_{s1}) = 0 \qquad (57)$$

where $n_{p1} = (EI\beta/L)_p \Big/ (EI\beta/L)_0$ and $(EI\beta/L_0)$ is the characteristic value chosen for the frame.

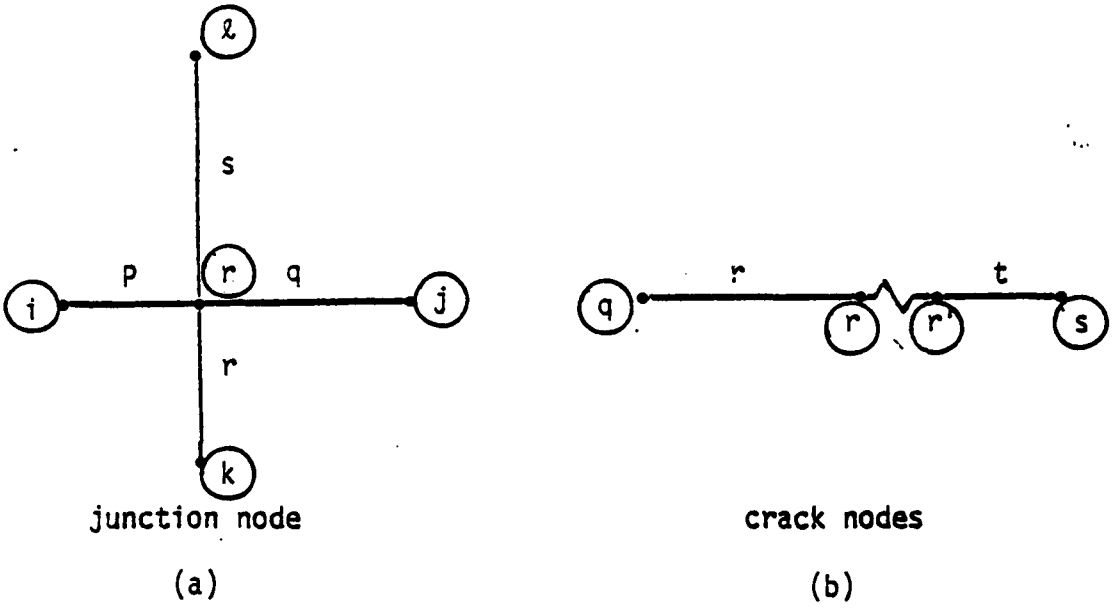


Figure 16. Typical Nodes on the Frame.

In the formulation of crack nodes, Figure 16b shows two nodes, r and r', across a crack on a beam element. Kirchhoff's current law is written for the node r:

$$(y'_q - y'_r)G_{ro} + (\bar{y}'_r - y'_r)(-\kappa) - y'_r G_r + I_{r2} = 0 \qquad (58)$$

where $y'_r$ is the rotation of the node r' and the conductance $-\kappa$ represents the crack. The nodal equation for the node r' is of a similar form. Equation (58) is valid whether the crack is on a girder or a column. Following the same steps which led to Equation (57) we may obtain

$$-y'_r(n_{r1}Q_r - \frac{1}{\theta\beta}) - \bar{y}'_r(\frac{1}{\theta\beta}) - y'_q n_{r1} W_r + \left(\frac{L}{EI\beta}\right)_0 I_{r2} = 0 \qquad (59)$$

Assemblage of the Nodal Equations:

From the small deformation theory, points on girders on the same floor level will have the same horizontal displacement. Namely,

$$y_{ij} = y_{n+i,j} = y_{2n+i,j} = \cdots = y_{mn+i,j} \qquad i = 1,\ldots,n \ , \quad j = 1,2 \qquad (60)$$

Also, $y_{i2} = y_{i+1,1}$, $i = 1,\ldots,n-1$. On the other hand, deflection continuity across a crack implies that deflections of the nodes r and r' in Figure 16b are equal. Thus, there are (n + k) unknown deflections associated with the frame, k denoting the total number of cracks on the frame. Designating by $y_i (y_i \equiv y_{i2}, i = 1,\ldots,n)$ the horizontal displacement of the ith floor, we obtain an (n + k) vector of displacements and an [n(m + 1) + 2k] -vector of rotations as

$$\underset{\sim}{y} \equiv \{y_1 \ \ y_2 \cdots y_n \ y_{n(2m+1)+1} \cdots y_{n(2m+1)+k}\}^T$$

$$\underset{\sim}{y}' \equiv \{y'_1 \cdots y'_{n(m+1)} \ \ y'_{n(2m+1)+1} \ \bar{y}'_{n(2m+1)+1} \ \cdots \bar{y}'_{n(2m+1)+k}\}^T \qquad (61)$$

where $y_{n(2m+1)+i}$ designates the transverse deflection at the ith crack, and $y'_{n(2m+1)+i}$ and $\bar{y}'_{n(2m+1)+i}$ designate the rotations immediately to the

left of (below) and to the right of (above) the ith crack which is on a girder (column). The unknown deflections can be related to the rotations via the kinetic equations, defining the sideway motion of the floors, and the shear continuity conditions at the cracks. Cross shears at the column ends are the axial driving forces for the floors [1, p. 42]. The axial acceleration of a floor, which is composed of all the girders on the same level, is the same as the transverse acceleration of the column ends at the nodes where the columns join the floor. Thus for the ith floor (Figure (17)

$$\sum_{j=0}^{m}\left[V_{jn+i,2} - V_{jn+i+1,1}\right] = \left\{\sum_{j=p}^{p+m-1} \rho_j L_j + \sum_{j=q}^{q+k_i-1} \rho_j L_j\right\}\omega^2 y_i \quad (62)$$

where $p = (m + 1)n + (i - 1)m + 1$ in accordance with the numbering order described earlier and $k_i$ is the total number of cracks on the ith floor. There is one such equation for each floor. The term in the braces on the right-hand side of Equation (62) is the total mass of the ith floor. Equation (62), upon substitution of the last two of Equations (19) for shears, will relate deflections to rotations. Figure 18b shows the diagram of a frame with $m = 1$, $n = 2$, $k = 2$. There are eight nodes, eight beam elements (hence eight interconnected $\Pi$ circuits) and four unknown deflections. The first floor has one crack on it. The kinetic equation for the first floor with $\rho_8 = \rho_5$, has the form

$$V_{12} + V_{32} - V_{21} - V_{71} = \omega^2 y_1 \rho_5 (L_5 + L_8) \quad (63)$$

where, for instance,

$$V_{32} = \frac{1}{h_3}(Q_3' y_3' - P_3 y_1 \beta_3 / L_3) \quad (64)$$

$$V_{71} = \frac{1}{h_7}[Q_7' y_3' + W_7' y_7' + (P_7 y_1 - P_7' y_7)\beta_7 / L_7]$$

from Equation (19) with $y_{31} = y_{31}' = 0$, $y_1 \equiv y_{32} = y_{71}$, $y_3' \equiv y_{32}' = y_{71}'$, $y_{72} = y_7$, $y_{72}' = y_7'$. Substituting shear expressions, Equations (64), and the similar equations for $V_{12}$ and $V_{21}$, into Equation (63) and rearranging, we obtain

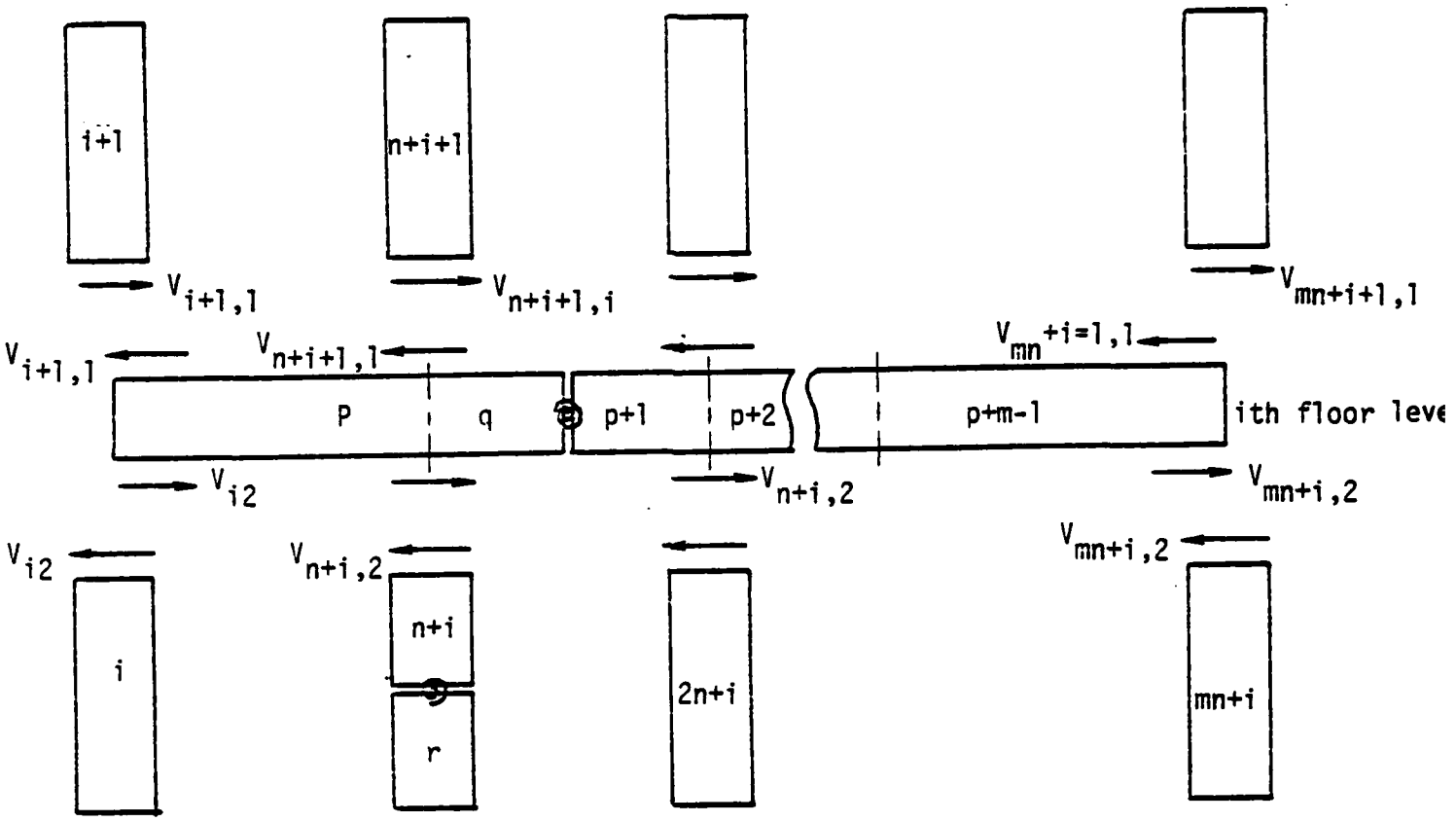


Figure 17. Cross Shears in the Columns Adjoining the ith Floor.

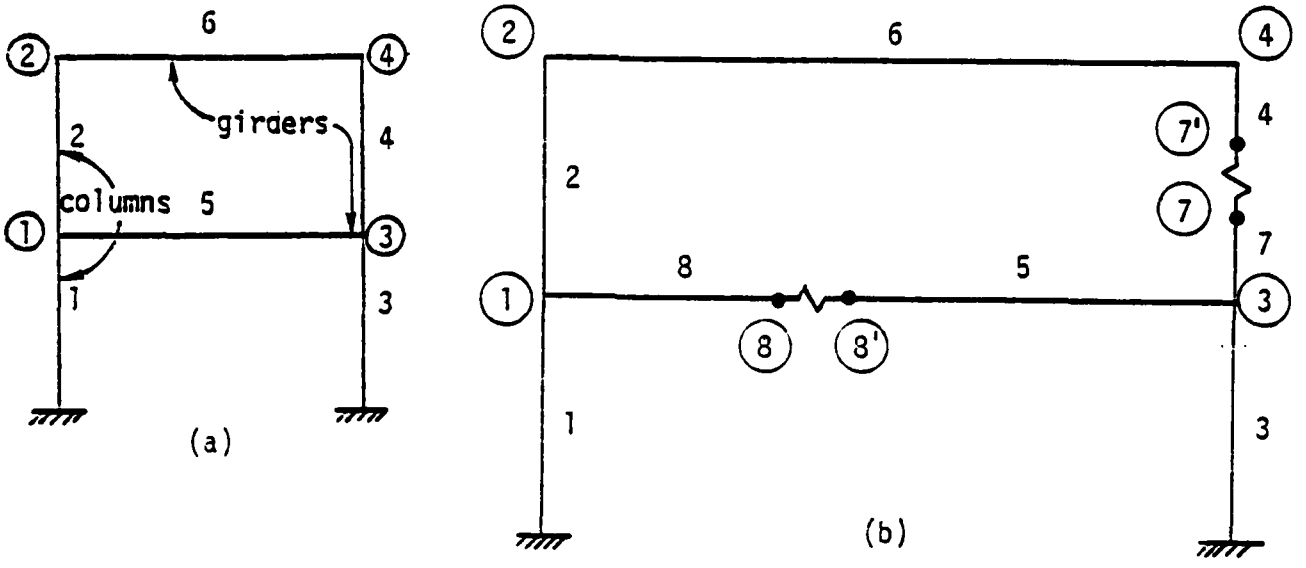


Figure 18. Two-story, Single Span Frame (a) with No Crack, (b) with Two Cracks.

$$\left(\frac{\beta}{L}\right)_0\Big\{[n_{13}P_1 + n_{23}P_2 + n_{33}P_3 + n_{73}P_7 + n_{53}(\beta_5 + \beta_8)]y_1$$

$$- n_{23}P_2'y_2 - n_{73}P_7'y_7\Big\} = (n_{12}Q_1' - n_{22}Q_2')y_1' - n_{22}W_2'y_2'$$

$$+ (n_{32}Q_3' - n_{72}Q_7')y_3' - n_{72}W_7'y_7' \qquad (65)$$

where

$$n_{ij} = (EI)_i(\beta_i/L_i)^j/[(EI)_0(\beta_0/L_0)^j] \quad . \qquad (66)$$

The kinetic equation for the second floor can be developed similarly. Application of shear continuity at a crack will now be demonstrated for the crack on the first floor (Fig. 18b). Hence $V_{82} = V_{51}$, or from the last two of Equations (19)

$$\frac{1}{h_8}(W_8'y_1' + Q_8'y_8' - P_8y_8\beta_8/L_8) = \frac{1}{h_5}(Q_5'\bar{y}_8' + W_5'y_3' + P_5y_8\beta_5/L_5) \qquad (67)$$

since $y_{81} = y_{52} = 0$. The following expression is obtained by rearranging Equation (67) and noting that $h_5 = h_8$ and $\beta_5/L_5 = \beta_8/L_8$:

$$\left(\frac{\beta_5}{L_5}\right)(P_5 + P_8)y_8 = W_8'y_1' - W_5'y_3' + Q_8'y_8' - Q_5'\bar{y}_8' \qquad (68)$$

For the general frame structure, there are n kinetic equations of the form of Equation (65) and k shear-continuiity equations of the form of Equation (68). These (n+k) equations can be arranged in a matrix form to solve for the deflections in terms of the rotations, namely,

$$\underset{\sim}{y} = \left(\frac{L}{\beta}\right)_0 \underset{\sim}{Z}^{-1}\underset{\sim}{X}\ \underset{\sim}{y}' \quad . \qquad (69)$$

On the other hand, the nodal equations (57) and (59) can be arranged in the form

$$\left(\frac{L}{EI\beta}\right)_0 \underset{\sim}{H}_1\underset{\sim}{I} - \underset{\sim}{U}\underset{\sim}{y}' = 0 \qquad (70)$$

where $\underset{\sim}{I}$ is the vector of current sources and is related to the deflections via Equations (23); that is,

$$\underset{\sim}{I} = \left(\frac{EI\beta^2}{L^2}\right)_0 \underset{\sim}{H}_2\underset{\sim}{y} \quad . \tag{71}$$

After Equation (69) is substituted into Equation (71), then Equation (71) into Equation (70), and it is noted that $\underset{\sim}{H}_1\underset{\sim}{H}_2 = \underset{\sim}{X}^T$, the slope equation results:

$$(\underset{\sim}{X}^T\underset{\sim}{Z}^{-1}\underset{\sim}{X} - \underset{\sim}{U})\underset{\sim}{y}' = \underset{\sim}{0} \quad . \tag{72}$$

This is the general form of the result for any planar frame with any number of cracks on it. The coefficient matrix in (72) is symmetric. The individual matrices, in general, have the forms

$$\underset{\sim}{X} = \begin{array}{c} \overbrace{\qquad\qquad\qquad\qquad}^{n(m+1)} \quad \overbrace{\quad}^{2k_c} \quad \overbrace{\quad}^{2k_g} \\ \left[\begin{array}{c|c|c|c} \underset{\sim}{X}^{(1)} & \cdots & \underset{\sim}{X}^{(m+1)} & \underset{\sim}{F}_c \quad \underset{\sim}{0} \\ \hline \underset{\sim}{E}_{c_1} & \cdots & \underset{\sim}{E}_{c,m+1} & \underset{\sim}{H}_c \quad \underset{\sim}{0} \\ \hline \underset{\sim}{E}_{g_1}' & \cdots & \underset{\sim}{E}_{g,m+1} & \underset{\sim}{0} \quad \underset{\sim}{H}_g \end{array}\right] \begin{array}{l} n \\ k_c \\ k_g \end{array} \end{array} \tag{73}$$

$$\underset{\sim}{U} = \begin{array}{c} \overbrace{\quad}^{n(m+1)} \quad \overbrace{\quad}^{2k_c} \quad \overbrace{\quad}^{2k_g} \\ \left[\begin{array}{c|c|c} \underset{\sim}{U}_0 & \underset{\sim}{A}_c & \underset{\sim}{A}_g \\ \hline \underset{\sim}{A}^T{}_c & \underset{\sim}{B}_c & \underset{\sim}{0} \\ \hline \underset{\sim}{A}^T{}_g & \underset{\sim}{0} & \underset{\sim}{B}_g \end{array}\right] \end{array} \quad \underset{\sim}{Z} = \begin{array}{c} \overbrace{\quad}^{n} \quad \overbrace{\quad}^{k_c} \quad \overbrace{\quad}^{k_g} \\ \left[\begin{array}{c|c|c} \underset{\sim}{Z}_0 & \underset{\sim}{C}_c & \underset{\sim}{0} \\ \hline \underset{\sim}{C}^T{}_c & \underset{\sim}{D}_c & \underset{\sim}{0} \\ \hline \underset{\sim}{0} & \underset{\sim}{0} & \underset{\sim}{D}_g \end{array}\right] \end{array} \tag{74}$$

with $\underset{\sim}{y}$ and $\underset{\sim}{y}'$ arranged as in Equation (61)

$$\underset{\sim}{y} = \{\underset{\sim}{y}_0 \quad \underset{\sim}{y}_c \quad \underset{\sim}{y}_g\}^T \quad , \quad \underset{\sim}{y}' = \{\underset{\sim}{y}'_0 \quad \underset{\sim}{y}'_c \quad \underset{\sim}{y}'_g\}^T \tag{75}$$

where the subscripts c and g refer to cracks on the columns and on the girders, respectively, with $k_c$ and $k_g$ being the total number of cracks on the columns and on the girders ($k = k_c + k_g$). It should be noted that $\underset{\sim}{X}^{(i)}$, $\underset{\sim}{U}_0$, and $\underset{\sim}{Z}_0$ for the case of no crack are modified when cracks are introduced on the frame. The matrices $\underset{\sim}{U}$ and $\underset{\sim}{Z}$ are symmetric. A formal procedure will now be described to establish the above matrices without the need to draw the actual analog circuit.

4.2 Procedure to Establish the Matrices

In the following, for simplicity of explanation, properties of the beam elements are assumed uniform throughout the frame, that is, $n_{ij} = 1$ for all i,j, except for the lengths. At the end, corrections for the general case are mentioned.

1. To establish the $\underset{\sim}{U}$ matrix:

$\underset{\sim}{U}$ is composed of the coefficients of the rotations $y_i'$ in equations such as (57) and (59). The ith row in the matrix stems from Kirchhoff's current law written for the ith node, the first n(m+1) rows being for the nodes on the frame joints and the next 2k rows for the nodes at the cracks. Hence,

a. the diagonal entry $u_{ii}$ will be the sum of the Q values, Equation (20), of the beam elements adjoining at the node for which Kirchhoff's current law is being written. If this node is at a crack, then $u_{ii}$ is given by the Q value of the element ending at this node minus the M value for the corresponding crack, where $M = 1/\beta\theta$. Diagonal entries of $\underset{\sim}{B}_c$ and $\underset{\sim}{B}_g$ will thus be of the form $(Q_t - M_r)$. And,

b. the off-diagonal entry $u_{ij}$ will be $W_k$, Equation (20), if the nodes corresponding to the columns i and j of the matrix are linked directly by the kth beam element. If these two nodes are linked by a crack, i.e., they are the nodes on the two sides of a crack, then $u_{ij}$ is given by the M value of the crack. Otherwise $u_{ij} = 0$. Due to symmetry, $u_{ij} = u_{ji}$. The ith row of $\underset{\sim}{U}_0$ in Equation (74) is unchanged relative to $\underset{\sim}{U}_0$ of the no-crack (k=0) case if the ith node is not adjacent to a cracked element.

2. To establish the $\underset{\sim}{Z}$ matrix:

The matrices $\underset{\sim}{Z}$ and $\underset{\sim}{X}$ stem from the kinetic equations and shear conditions. The first n rows in them represent the kinetic equations governing side sway of the n floors. The last k rows correspond to shear continuity conditions at the cracks. $\underset{\sim}{Z}$ consists of the coefficients of deflections $y_i$ and its entries can be generated as follows:

a. The diagonal entry $z_{ii}$ for i=1,2,...n will be the sum of the $\beta_k$ values of all the girder elements on the ith floor plus the sum of the P values, Equation (20), of all the columns adjoining at the ith floor. If a column adjacent to the ith floor is cracked, then only the P value of the column segment nearest to that floor will be included. $\beta_k$ can be expressed in terms of the characteristic value $\beta_0$ as $\beta_k = e_k\beta_0$. If the frame is homogeneous in properties, then $e_k = L_k/L_0$. Diagonal entries $z_{ii}$ for the last k rows (i.e., diagonal entries of the $\underset{\sim}{D}$ matrices) will be the sums of the P values of the two beam segments on the two sides of the corresponding crack.

b. The off-diagonal entry $z_{i,i+1}$ of $\underset{\sim}{Z}_0$ will be the negative of the sum of the P' values, Equation (20), of all uncracked columns joining ith and (i+1)th floors. $z_{i,i+1} = 0$ if all the columns between those floors are cracked. $z_{ij} = 0$ for $n \geq j \geq i+2$ and $z_{ij} = z_{ji}$. $\underset{\sim}{Z}_0$ is, hence, a tridiagonal symmetric matrix. If any one of the columns adjacent to the ith floor is cracked, then $z_{ij}$ for $1 \leq i \leq n$, $n < j \leq n + k_c$ (i.e., entries of $\underset{\sim}{C}_c$), will be zero except for that (those) j value(s) which correspond(s) to the deflection(s) at the crack(s) nearest to the ith floor, in which case $z_{ij}$ is equal to the negative of the P' value for the column segment which links the ith floor to that crack. If none of the columns adjacent to ith floor is cracked, then ith row of $\underset{\sim}{C}_c$ is zero and the ith row of $\underset{\sim}{Z}_0$ is unchanged relative to $\underset{\sim}{Z}_0$ of the no-crack (k=0) case.

$z_{i,i+1}$ for $n < i \leq + k_c$ (entries of $\underset{\sim}{D}_c$) will be zero if there is no other crack between the (i-n)th column crack and the floor level above

this crack. Otherwise, $z_{i,i+1}$ will be equal to the negative of the P' value for the column segment which links the (i-n)th and the (i-n+1)st cracks.

$z_{i,i+1}$ for $n+k_c < i \leq n + k_g$ (entries of $\underset{\sim}{D}_g$) will be zero if there is no other crack between (i-n-$k_c$)th girder crack and the wall to the right of this crack. Otherwise $z_{i,i+1}$ will be equal to the negative of the P' value for the girder segment which links the (i-n-$k_c$)th crack and the crack on its right.

Hence, $\underset{\sim}{D}_c$ and $\underset{\sim}{D}_g$ are diagonal if at most one crack exists on each beam element. If more than one crack exists on any column or girder, then $\underset{\sim}{D}_c$ and/or $\underset{\sim}{D}_g$ are accordingly tridiagonal symmetric matrices.

3. To establish the $\underset{\sim}{X}$ matrix:

$\underset{\sim}{X}$ consists of the coefficients of rotations $y_i'$ in equations such as (65) and (68). A square submatrix $\underset{\sim}{X}^{(k)}$ in Equation (73) corresponds to rotations of the frame joints on the kth wall (Fig. 15).

a. The diagonal entry $x_{ii}^{(k)}$, which stems from the kinetic equation for the ith floor, will be given by the Q' value, Equation (20), of the column (column segment) under the frame-joint node n(k-1)+i minus the Q value of the column (column segment) above the same node. If there is no cracked column on the kth wall, then $x_{ii}^{(k)} = Q'_{n(k-1)+i} - Q'_{n(k-1)+i+1}$ for i=1,...,n-1 and $x_{nn}^{(k)} = Q'_{nk}$.

b. The off-diagonal entry $x_{i,i+1}^{(k)} = -W'_{n(k-1)+i+1}$ (that is, the negative of the W' value, Equation (20), for the column above node n(k-1)+i) for i=1,...n-1 if the column of the kth wall between the ith and (i+1)th floors (i.e., the column above node n(k-1)+i) has no crack on it. Otherwise $x_{i,i+1}^{(k)} = 0$, and that entry on the ith row of $\underset{\sim}{F}_c$ which corresponds to the rotation of the crack node nearest to and above the node n(k-1)+i will be equal to the negative of the W' value of the column segment linking the node n(k-1)+i and the said crack node. $x_{ij}^{(k)} = 0$ for $j \geq i+2$ and $x_{ij}^{(k)} = -x_{ji}^{(k)}$ for $i \neq j$. (Entries of each $\underset{\sim}{X}^{(k)}$ are numbered independently of the other submatrices.) $\underset{\sim}{X}^{(k)}$ is thus diagonal if each column of the kth wall has at least one crack. Otherwise it is

tridiagonal. $\underset{\sim}{X}^{(k)}$ is unchanged relative to $\underset{\sim}{X}^{(k)}$ of the no-crack (k=0) case if there is no crack on the kth wall.

If the column below node n(k-1)+i is cracked, then that entry on the ith row of $\underset{\sim}{F}_c$ which corresponds to the rotation of the crack node nearest to and below the node n(k-1)+i will be equal to the W' value of the column segment linking the two nodes. Except for this and the above mentioned cases, entries of $\underset{\sim}{F}_c$ are zero.

c. The $\underset{\sim}{E}$ matrices in Equation (73) couple the crack nodes with the frame-joint nodes. Rows n+1 through n+k of $\underset{\sim}{X}$ (i.e., $\underset{\sim}{E}$ and $\underset{\sim}{H}$ matrices) are filled in as follows: The entry on the matrix column which corresponds to rotation of the node on the left (or lower) side of the crack, at which the shear continuity condition is being written, is equal to the Q' value of the girder (or column) segment which links this node to the one on its left (or below it). The entry corresponding to the node on the right (or upper) side of the crack is equal to minus the Q' value of the segment linking this node to the node on its right (or above it). These two entries are within the submatrix $\underset{\sim}{H}_g$ (or $\underset{\sim}{H}_c$). The entry, corresponding to the node on the left of (or below) the left (or lower) crack-node, is equal to the W' value of the segment linking these two nodes. Finally, the entry corresponding to the node on the right of (or above) the right-side (or upper) crack-node is equal to the negative of the W' value of the segment linking the two nodes. These two entries can be within the submatrices $\underset{\sim}{E}$ or $\underset{\sim}{H}$ depending on whether there are one or more cracks on a girder (column). $\underset{\sim}{E}_{c,k} = \underset{\sim}{0}$ if there is no crack on the kth wall; $\underset{\sim}{E}_{g,k} = \underset{\sim}{0}$ if there is no crack on any of the girders adjacent to the kth wall.

4. Corrections for the general case:

If beam properties are not uniform throughout the frame (each column or girder still has uniform properties within itself), then the following corrections are necessary:

a. Multiply each term in the $\underset{\sim}{U}$ matrix, except the terms of the form $1/\beta\theta_\ell$, by the corresponding $n_1$ value, that is, $Q_p$ and $W_p$ by $n_{p1}$.

b. Multiply each term in the first n rows of the $\underset{\sim}{X}$ matrix by the corresponding $n_2$ value, that is, $Q_p'$ and $W'_p$ by $n_{p2}$.

c. Multiply each term in the first n rows of the $\underset{\sim}{Z}$ matrix by the corresponding $n_3$ value, that is, $P_p$ and $P_p'$ by $n_{p3}$ and $\beta_r$ by $n_{r3}$.

d. Multiply the ith row of $\underset{\sim}{Z}$, $n+1 \leq i \leq n+k$, by $(\beta_\ell/L_\ell)/(\beta_0/L_0)$ where $\ell$ is the number of the element on which the crack for which the ith row represents the shear continuity condition is located.

The above procedure will now be illustrated with an example.

Example 1. The illustrated frame is depicted in Figure 18.

a. Frame without cracks (Fig. 18a) with different beam properties.

$$\begin{array}{c} \quad y_1' \qquad\qquad y_2' \qquad\qquad y_3' \qquad\qquad y_4' \\ \underset{\sim}{U} = \begin{bmatrix} n_{11}Q_1+n_{21}Q_2+n_{51}Q_5 & n_{21}W_2 & n_{51}W_5 & 0 \\ n_{21}W_2 & n_{21}Q_2+n_{61}Q_6 & 0 & n_{61}W_6 \\ n_{51}W_5 & 0 & n_{31}Q_3+n_{41}Q_4+n_{51}Q_5 & n_{41}W_4 \\ 0 & n_{61}W_6 & n_{41}W_4 & n_{41}Q_4+n_{61}Q_6 \end{bmatrix} \end{array} \tag{76}$$

$$\begin{array}{c} \quad y_1 \qquad\qquad\qquad y_2 \\ \underset{\sim}{Z} = \begin{bmatrix} n_{13}P_1+n_{23}P_2+n_{33}P_3+n_{43}P_4+n_{53}\beta_5 & -n_{23}P_2'-n_{43}P_4' \\ -n_{23}P_2' - n_{43}P_4' & n_{23}P_2+n_{43}P_4+n_{63}\beta_6 \end{bmatrix} \end{array} \tag{77}$$

$$\begin{array}{c} \quad y_1' \qquad\quad y_2' \qquad\quad y_3' \qquad\quad y_4' \\ \underset{\sim}{X} = \begin{bmatrix} n_{12}Q_1'-n_{22}Q_2' & -n_{22}W_2' & n_{32}Q_3' -n_{42}Q_4' & -n_{42}W_4' \\ n_{22}W_2' & n_{22}Q_2' & n_{42}W_4' & n_{42}Q_4' \end{bmatrix} \end{array} \tag{78}$$

where, for convenience, the rotations and the deflections at the nodes are written above the corresponding columns of the matrices. The $\det(\underline{X}^T\underline{Z}^{-1}\underline{X}-\underline{U})$ then yields the modal frequencies of the frame without crack.

b. Frame with two cracks (Fig. 18b). The frame is now assumed uniform. Hence, $n_{ij}=1$ and $e_\ell=\beta_\ell/\beta_0=L_\ell/L_0$.

$$\underline{U} = \begin{array}{c} \begin{array}{cccc|cccc} y_1' & y_2' & y_3' & y_4' & y_7' & \bar{y}_7' & y_8' & \bar{y}_8' \end{array} \\ \left[\begin{array}{cccc|cccc} Q_1+Q_2+Q_8 & W_2 & 0 & 0 & 0 & 0 & W_8 & 0 \\ W_2 & Q_2+Q_6 & 0 & W_6 & 0 & 0 & 0 & 0 \\ 0 & 0 & Q_3+Q_5+Q_7 & 0 & W_7 & 0 & 0 & W_5 \\ 0 & W_6 & 0 & Q_4+Q_6 & 0 & W_4 & 0 & 0 \\ \hline 0 & 0 & W_7 & 0 & Q_7-M_4 & M_4 & 0 & 0 \\ 0 & 0 & 0 & W_4 & M_4 & Q_4-M_4 & 0 & 0 \\ W_8 & 0 & 0 & 0 & 0 & 0 & Q_8-M_5 & M_5 \\ 0 & 0 & W_5 & 0 & 0 & 0 & M_5 & Q_5-M_5 \end{array}\right] \end{array} \tag{79}$$

It may be noted that the first four elements in the second row of $\underline{U}$ are the same as those in the second row in Equation (76) (except for the factors $n_{p1}$ . This row is unchanged since node 2 is not linked to any crack node. If the beams had different properties, then each term in $\underline{U}$ would be multiplied by the corresponding $n_1$ value except the terms $M_\ell = 1/\beta\theta_\ell$. In the $M_\ell$ terms, the sensitivity numbers, $\theta_\ell$, are subscripted by the original number of the column or girder on which the corresponding cracks are located. Hence, $\theta_4$, for instance, refers to the crack located on the column numbered 4 in the uncracked frame (Fig. 18). It is also noted that $Q_4$, $W_4$, $P_4$, etc. for the cracked frame have different values from the ones in the no-crack case. The $\underline{Z}$ and $\underline{X}$ matrices of the cracked frame are subsequently conjugated as:

$$
\underset{\sim}{Z} = \begin{array}{c} \begin{matrix} y_1 & & y_2 & & y_7 & y_8 \end{matrix} \\ \left[\begin{array}{cc|cc} P_1+P_2+P_3+P_7+\beta_5+\beta_8 & -P_2' & -P_7' & 0 \\ -P_2' & P_2+P_4+\beta_6 & -P_4' & 0 \\ \hline -P_7' & -P_4' & P_4+P_7 & 0 \\ 0 & 0 & 0 & P_5+P_8 \end{array}\right] \end{array} \tag{80}
$$

$$
\underset{\sim}{X} = \begin{array}{c} \begin{matrix} y_1' & y_2' & y_3' & y_4' & y_7' & \bar{y}_7' & y_8' & \bar{y}_8' \end{matrix} \\ \left[\begin{array}{cc|ccc|cc|cc} Q_1' & -Q_2' & -W_2' & Q_3' & -Q_7' & 0 & -W_7' & 0 & 0 & 0 \\ W_2' & Q_2' & & 0 & Q_4' & 0 & W_4' & 0 & 0 & \\ \hline 0 & 0 & & W_7' & -W_4' & Q_7' & & -Q_4' & 0 & 0 \\ W_8' & 0 & & -W_5' & 0 & 0 & & 0 & Q_8' & -Q_5' \end{array}\right] \end{array} \tag{81}
$$

where $\underset{\sim}{X}^{(1)}$ in Equation (78) and Equation (81) are basically the same since there is no crack on the first wall. The terms $-W_4'$ and $W_4'$ in $\underset{\sim}{X}^{(2)}$ in Equation (78) are replaced by zeros in Equation (81), since nodes 3 and 4 are no longer linked directly. As the column under the node 4 is cracked, the node 4 is now linked to the node 7' by the column segment 4. Therefore, $W_4'$ appears on the second row and second column (which corresponds to $\bar{y}_7'$) of $\underset{\sim}{F}_c$. The third row of $\underset{\sim}{X}$ reflects the continuity of shear at the column crack in Figure 18b. The lower crack-node 7 is linked to the node 3 by the column segment 7 and the upper crack-node 7' is linked to the node 4 by the segment 4. Q' and W' values are accordingly placed on the third row. The construction of the matrices for the cracked frame is now complete.

Figure 19 illustrates the relative changes in the first three natural frequencies of a two-story single-span frame with a single crack of $\theta = .174$. The frame has uniform properties (i.e., $n_{ij} = 1$ for all i,j) and all six of the beam elements are of equal length, (i.e., $\beta_i$ are the same for all the six elements). Due to symmetry, a crack on element 3 or

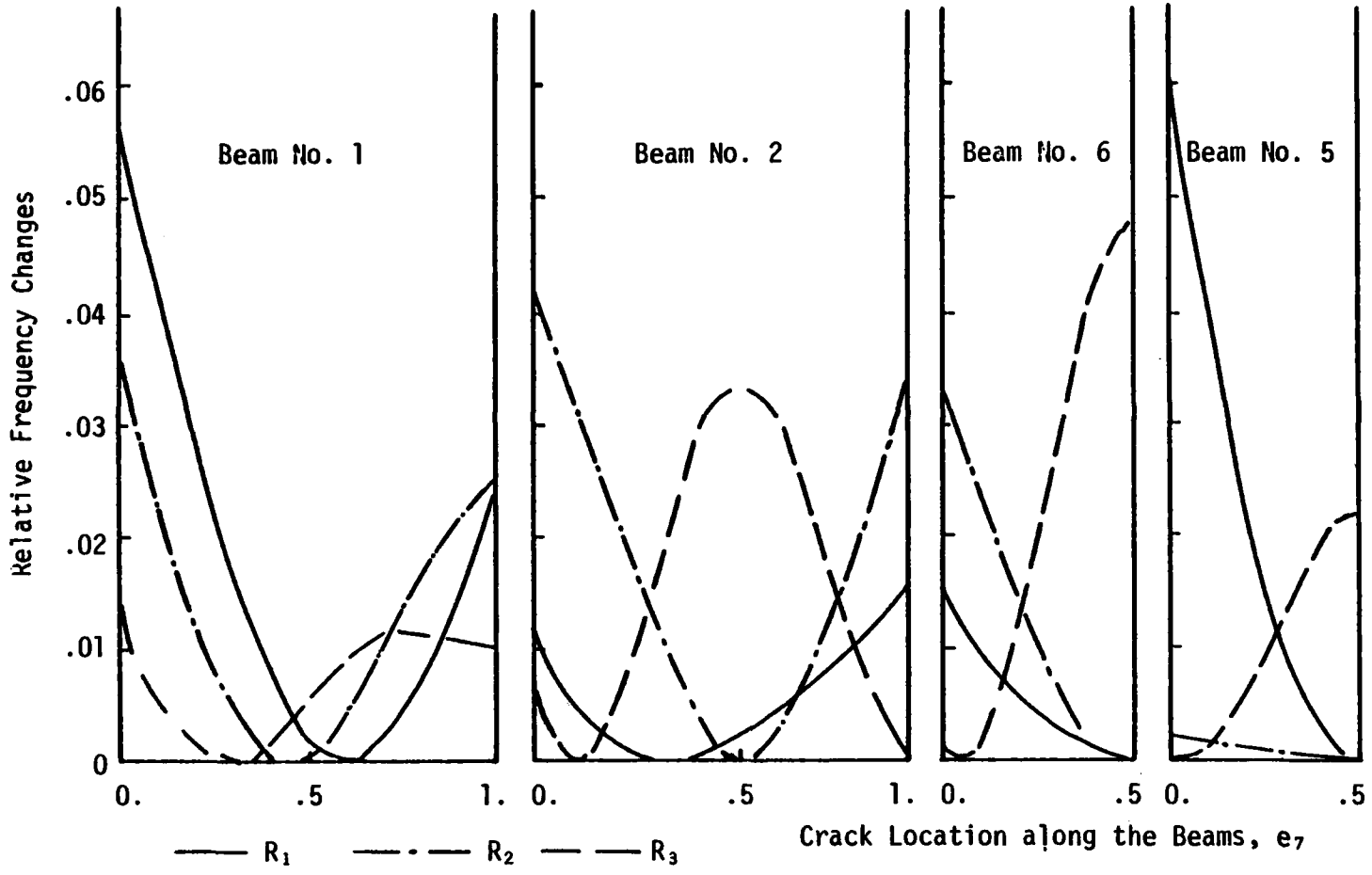


Figure 19. Two-story Single-span Uniform Frame with a Single Crack of $\theta = 0.174$: Relative Frequency Changes as a Function of Crack Location.

4 will yield the same R curves as a similar crack on element 1 or 2, respectively (Fig. 18a). The first three characteristic values for such a frame with no crack are $\beta^{(1)} = 1.2240$, $\beta^{(2)} = 2.2177$, $\beta^{(3)} = 3.2885$. Similar to the guidelines established previously for damage diagnosis on a cantilever beam, the following conclusions can be deduced from Figure 19 for the specific frame involved. (Due to symmetry, only the left half of the frame need be considered).

a. In cases when $R_1$ is relatively large and $R_2$ and $R_3$ have near-zero values, the (major) crack is either on the column element 1 at a distance of 0.35-0.40 from the ground or on the girder element 5 at a distance of 0.0-0.15 from the corner, or there are two major cracks, one each at the given locations.

b. In cases when $R_2$ is relatively large and $R_1$ and $R_3$ are near zero, the crack is on the column element 2 at 0.15-0.20 distance from the lower joint.

c. For the case when $R_3$ is relatively large and $R_1$ and $R_3$ are small, the crack is on element 2 at $e_7 = 0.45$-$0.60$, or near the mid-point of either of the girders, or there may be a major crack at each of these locations.

d. When $R_1$ is very small and both $R_2$ and $R_3$ are relatively large and have comparable values (say, different by no more than 0.01 at the range of values in Figure 19), the crack(s) is (are) on element 1 at $e_7 = 0.55$-$0.65$ and/or an element 2 at $e_7 = 0.25$-$0.40$.

e. In the case when $R_2$ is very small and $R_1$ and $R_3$ are both large and comparable in value, the crack(s) may be on element 1 at $e_7 = 0.40$-$0.50$ and/or on element 5 at $e_7 = 0.25$-$0.35$. However, there are other possibilities, an example of which is the presence of three major cracks, one each on element 1 at $e_7 = 0.4$-$0.5$, on element 2 at $e_7 = 0.5$-$0.6$, and on element 5 at $e_7 = 0.0$-$0.20$.

f. If all $R_j$ are comparable in value, many possibilities exist. The above guidelines (for equal-legged frame) are reasonable estimates. They illustrate the use of relative $R_j$ values when a numerical solution cannot be found for a single crack. They also serve the direction of probabilistic measure to be developed later.

Example 2.

The first three characteristic values $\beta_u$ for an undamaged two-story single-span uniform frame of equal-length elements are 1.2240, 2.2177, and 3.2885. The following relative frequency changes have been computed from the measured frequencies of a damaged frame of such characteristics: $R_1$= 0.011, $R_2$ = 0.025, $R_3$ = 0.005. The damage will be estimated based on these relative changes.

The characteristic values for the damaged frame are computed from Equation (54). The first two of these values are used in the inverse problem with k=1 (section 3.2); that is, a solution for a single (major) crack is sought. Four possible damage pairs are thus computed; namely,

$(e_7, \theta_1) = (0.811, 0.278)$
$(e_7, \theta_6) = (0.094, 0.191)$

and due to symmetry

$(e_7, \theta_3) = (0.811, 0.278)$
$(e_7, \theta_6) = (0.906, 0.191)$

where $e_7 = L_7/L$ indicates relative crack location measured from the lower end of each column or the left-hand end of each girder. The subscripts "eq" for equivalent which were used in Chapter 3 have been dropped here. The subscript on $\theta$ indicates the structure element on which the crack is located. The major crack is thus either on one of the first story columns (i.e., on column 1 or 3) or on the second floor girder (i.e., beam number 6) (Fig. 18a). To decide where the actual crack is located, $(e_7, \theta_1)$ and $(e_7, \theta_6)$ are each used separately in the forward problem to compute the relative reduction in the third natural frequency which would be caused by each crack alone. The computed values are 0.017 and 0.002,

respectively. The second value is closer to the actual measured $R_3$ value of 0.005. Thus, it may be concluded that the crack is on the second floor girder, i.e., on element 6. The fact that the actual $R_3$ value is greater than the computed value may be due to a minor crack on the frame, for example, near the middle of girder 5 or 6 (Fig. 19). It must be stressed, however, that one major crack is assumed to exist in the above computations. The same $R_j$ values may be produced by a combination of minor cracks or, for instance, by two major cracks, one on column 1 at 0.40-0.50, the other on girder 6 at 0.05-0.10 (Fig. 19). In the latter case, the crack on column 1 would, by itself, produce almost no change in the second natural frequency while rendering small changes (<0.003) in the fundamental and third frequencies. The crack on girder 6 would, on the other hand, produce negligible change in the third frequency while causing changes greater than 1% in the other two frequencies. The effects of cracks are, by no means, linearly additive. Qualitatively, however, a certain crack contributes most to the decrease of that frequency which would experience the largest decrease if that particular crack were the only one present on the structure. This trend was illustrated by Example 5 on a cantilever beam in the previous chapter. The uncertainty of damage diagnosis emerges from the measurability of only a few frequencies of a structure.

Damage diagnosis can be highly sensitive to $R_j$ values at certain locations of the $R_j$ curves. If, for example, $R_1$ is measured to be 0.010 instead of 0.011 in this example, then the possible damage pairs will be

$$(e_7, \theta_1) = (0.795, 0.299) \quad ; \quad R_{3eq} = 0.018$$
$$(e_7, \theta_6) = (0.295, 0.963) \quad ; \quad R_{3eq} = 0.094$$

together with their symmetrical counterparts.

There is a considerable change in the second pair while the first is affected only slightly. In this case, the first pair would be selected as the likely diagnosis since $R_{3eq}$ is closer to the measured value of 0.005.

## 5. CONCLUSION

In a previous report, damage diagnosis in simple structures was studied [1]. In this report, analogy between beams and simple electrical circuits has been utilized to extend the modal method of diagnosis to multiple cracks and more complex frame structures. Computation of modal frequencies of an n-story m-span frame with k cracks (the forward problem) requires inverting a matrix (or, equivalently, solving a linear system) of order (n+k) and finding zeros of a deteminant of order [n(m+1) + 2k]. In finite element methods, using generally 20 elements per basic beam segment, there are slightly less than 20n(2m+1) nodes each with two degrees of freedom. The size of computation savings with analog circuits is almost 40-fold. However, using circuit analogy in determining the location and intensity of a crack (the inverse problem of diagnoses with k=1) may involve n(2m+1) computations of zeros of a determinant of order [n(m+1) + 2] while inverting a matrix of order (n+1) each time, since the crack can be on any one of the n(2m+1) elements of the frame. On the other hand, modal frequencies of a cantilever beam with k cracks can be computed with analog T circuits by inverting a matrix and finding zeros of a determinant, both of the order (k+1).

It is shown, in the report, that closely spaced multiple cracks can be effectively represented by a single crack for which the sensitivity number $\theta$ is approximately equal to the sum of the individual sensitivity numbers. Uncertainty exists, however, in diagnosing such a damage as to whether there is only one major crack or several closely spaced minor cracks. Nevertheless, location of the damage can be identified quite accurately.

In the case of a structure with several cracks, only one of which is severe, it is possible to diagnose the major crack. The contributions of minor cracks to frequency decreases is small compared to that of the severe crack. The relative frequency changes, $R_j$, in such a situation, exhibit a trend similar to that which would be observed were the major crack the only crack present on the structure. If there is more than one major crack, not closely spaced, on the structure, it is, in general, not possible to diagnose deterministically the damage with only three $R_j$

values known, although the minimum number of cracks may be estimated. Currently, the effect of damping is being investigated as a means to render diagnosis of such damage. Curves of relative frequency changes, $R_j$ versus crack location yield valuable information regarding damage diagnosis. It may be psssible to estimate damage location, provided there is only one major crack, by only looking at the relative magnitudes of frequency decreases and using the relative-change curves. The process may be tedious for more complex structures. Nevertheless, such curves can be of qualitative help to the numerical results. However, when cross-over occurs in the modal frquencies, $R_j$ curves cannot be used unless the correspondence between the pre-and post-damage frequencies is known. The approach described in Section 3.2 eliminates the effect of the cross-over problem on diagnosis of a major crack by eliminating the need to know this correspondence.

In diagnosing damage in a structure, given three post-damage characteristic values, $\beta$, the solution is sought for a single crack since there are not enough equations to solve for a larger number of cracks. It is shown that the same $\beta$ values can be produced by one crack or a combination of several cracks. Consideration must then be given to whether it is more likely, during a strong motion event, to produce a few major cracks or several minor cracks. In solving for a single crack, (i.e., for $e_{eq}$ and $\theta_{eq}$) two measured $\beta$ values are actually used first. The third measured $\beta$ value is then compared with the computed counterpart, which would be produced by the crack with the characteristic pair $(e_{eq},\theta_{eq})$. It is shown that the two $\beta$ values may not match closely even though the diagnosis is accurate (that is, $e_{eq}$ and $\theta_{eq}$ identify the major crack correctly), the discrepancy possibly being due to the presence of other minor cracks. If the discrepancy is large, then the solution is rejected with the conclusion that there is more than one major crack. On the other hand, the choice of the pair of measured $\beta$ values to be used in computing $e_{eq}$ and $\theta_{eq}$ may affect the diagnosis. In some cases, choosing the two characteristic values which correspond to the largest two $R_j$ values leads to the correct diagnosis. It is not clear, however, what the right choice is in each case.

Finally, for frame structures, the change in frequencies due to cracks is relatively small. Furthermore, damage diagnosis can be highly sensitive to $R_j$ values in certain cases. Therefore, accuracy in field measurement of the structural response is of extreme importance.

## REFERENCES


1. Ju, F. D., Akgun, M., Paez, T. L., and Wong, E. T., "Diagnosis of Fracture Damage in Simple Structures," Technical Report CE-62(82)AFOSR-993-1.

2. Keropyan, K. K., and Chegolin, P. M., Electrical Analogues in Structural Engineering, Edward Arnold (Publishers) Ltd., 1967.

## APPENDIX

1. T-Circuit Equations:

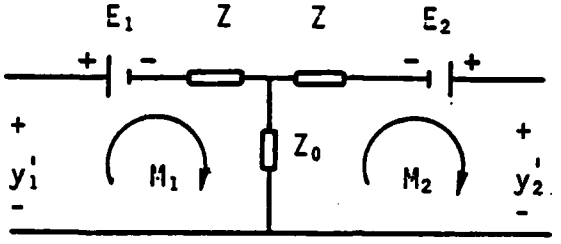


In this part, the circuit equations which relate the input-output voltages ($y_1'$, $y_2'$) of a T circuit to the input-output currents ($M_1$, $M_2$) are developed. The terms input and output refer to the left and right ports of the circuit in the figure and are used in a relative sense. In Figure 2 in the text, the currents $M_1$ and $M_2$ were shown at the branches of the circuit (as input and output currents) whereas in the above figure they are shown as mesh currents. In principle, there is no difference between the two. However, the latter is conceptually more helpful in developing the circuit equations.

The two sides of the circuit in the figure can be considered as meshes. The sum of the voltages around each mesh is equal to zero (Kirchhoff's voltage law). Hence,

$$E_1 + (Z + Z_0)M_1 - Z_0M_2 - y_1' = 0$$
$$-E_2 + (Z + Z_0)M_2 - Z_0M_1 + y_2' = 0$$

where E and Z are the voltage source and impedance, respectively.

These equations can be solved for the voltages; that is,

$$y_1' = (Z + Z_0)M_1 - Z_0M_2 + E_1$$
$$y_2' = Z_0M_1 - (Z + Z_0)M_2 + E_2$$

which are the same as Equations (8) in the text.

2. Π-Circuit Equations:

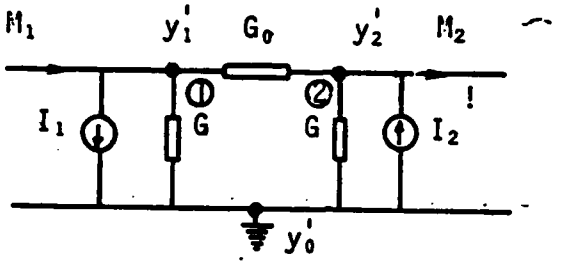


In this circuit, there are two nodes, with node voltages $y_1'$ and $y_2'$, and a reference node, $y_0'$ which is assigned a zero voltage. G and $G_0$ are conductances and $I_1$ and $I_2$ are current sources. The sum of the currents entering each node is zero (Kirchhoff's current law). Hence, for nodes 1 and 2

$$M_1 - I_1 - G(y_1' - y_0') - G_0(y_1' - y_2') = 0$$
$$-M_2 + I_2 - G(y_2' - y_0') - G_0(y_2' - y_1') = 0 \quad .$$

The term $G_0(y_1' - y_2')$, for instance, denotes the current flowing through the conductance $G_0$ from the node 1 to the node 2. There is a minus sign in front of the term since, in the first equation, currents entering the first node are taken to be positive. The equations can be solved for the currents $M_1$ and $M_2$; hence, with $y_0' = 0$,

$$M_1 = (G + G_0)y_1' - G_0y_2' + I_1$$
$$M_2 = G_0y_1' - (G + G_0)y_2' + I_2$$

which are the same as Equations (21) in the text.

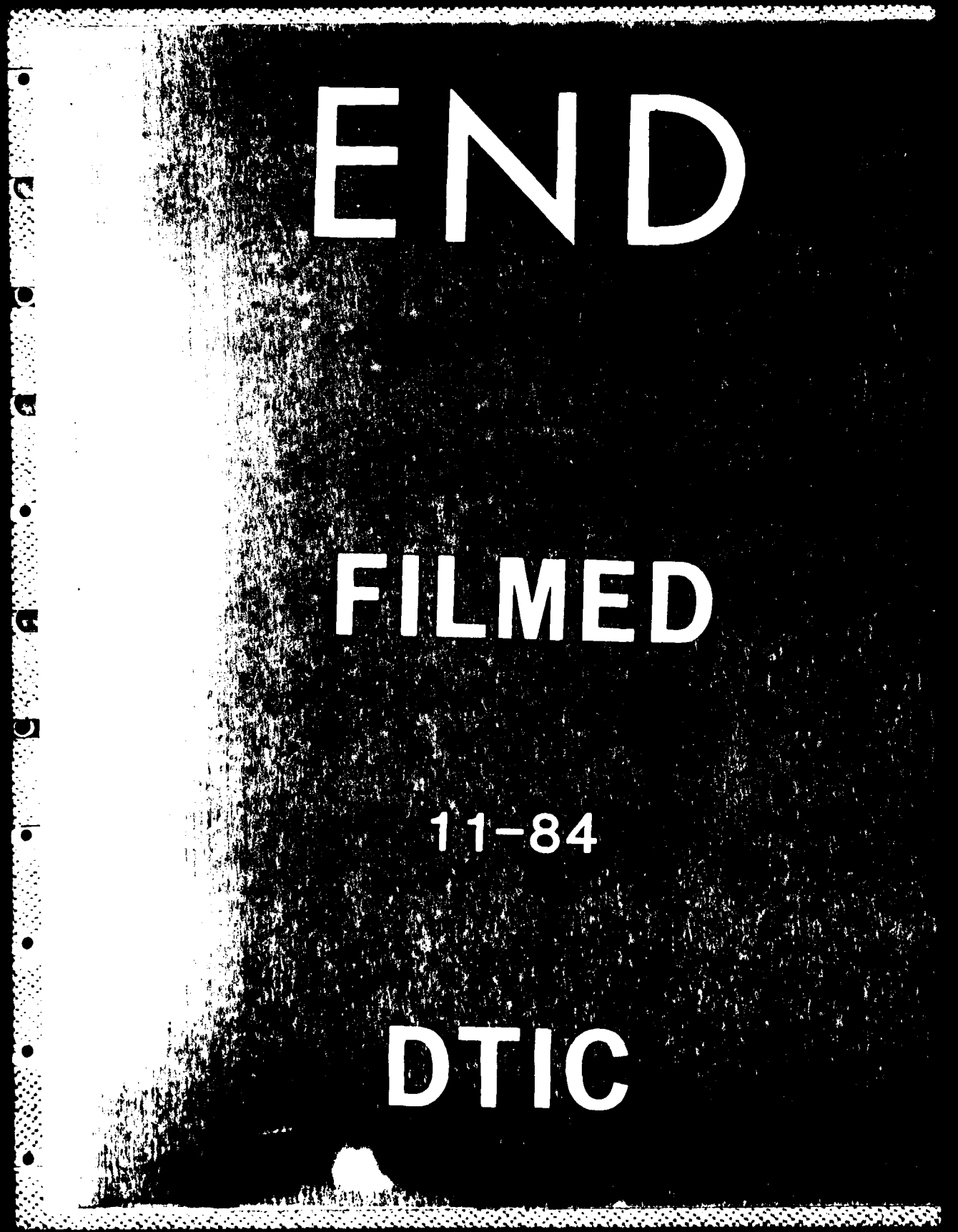
END
FILMED
11-84
DTIC